

# 1 Superiorization: An optimization heuristic for medical physics

2 Gabor T. Herman\*

3 *Department of Computer Science, The Graduate Center,*  
4 *City University of New York, New York, NY 10016, USA*

5 Edgar Garduño

6 *Departamento de Ciencias de la Computación,*  
7 *Instituto de Investigaciones en Matemáticas Aplicadas y en Sistemas,*  
8 *Universidad Nacional Autónoma de México,*  
9 *Cd. Universitaria, C.P. 04510, Mexico City, Mexico*

10 Ran Davidi

11 *Department of Radiation Oncology, Stanford University, Stanford, CA 94305, USA*

12 Yair Censor

13 *Department of Mathematics, University of Haifa, Mt. Carmel, 31905 Haifa, Israel*

14 **Purpose:** To describe and mathematically validate the superiorization methodol-  
15 ogy, which is a recently-developed heuristic approach to optimization, and to discuss  
16 its applicability to medical physics problem formulations that specify the desired  
17 solution (of physically given or otherwise obtained constraints) by an optimization  
18 criterion.

19 **Methods:** The superiorization methodology is presented as a heuristic solver for  
20 a large class of constrained optimization problems. The constraints come from the  
21 desire to produce a solution that is constraints-compatible, in the sense of meeting  
22 requirements provided by physically or otherwise obtained constraints. The underly-  
23 ing idea is that many iterative algorithms for finding such a solution are perturbation  
24 resilient in the sense that, even if certain kinds of changes are made at the end of  
25 each iterative step, the algorithm still produces a constraints-compatible solution.  
26 This property is exploited by using permitted changes to steer the algorithm to a  
27 solution that is not only constraints-compatible, but is also desirable according to  
28 a specified optimization criterion. The approach is very general, it is applicable to

29 many iterative procedures and optimization criteria used in medical physics.

30 **Results:** The main practical contribution is a procedure for automatically pro-  
31 ducing from any given iterative algorithm its superiorized version, which will supply  
32 solutions that are superior according to a given optimization criterion. It is shown  
33 that if the original iterative algorithm satisfies certain mathematical conditions, then  
34 the output of its superiorized version is guaranteed to be as constraints-compatible as  
35 the output of the original algorithm, but it is superior to the latter according to the  
36 optimization criterion. This intuitive description is made precise in the paper and  
37 the stated claims are rigorously proved. Superiorization is illustrated on simulated  
38 computerized tomography data of a head cross-section and, in spite of its general-  
39 ity, superiorization is shown to be competitive to an optimization algorithm that is  
40 specifically designed to minimize total variation.

41 **Conclusions:** The range of applicability of superiorization to constrained opti-  
42 mization problems is very large. Its major utility is in the automatic nature of  
43 producing a superiorization algorithm from an algorithm aimed at only constraints-  
44 compatibility; while non-heuristic (exact) approaches need to be redesigned for a new  
45 optimization criterion. Thus superiorization provides a quick route to algorithms for  
46 the practical solution of constrained optimization problems.

47 Keywords: superiorization, constrained optimization, heuristic optimization, tomography,  
48 total variation

## 49 I. INTRODUCTION

50 Optimization is a tool that is used in many areas of Medical Physics. Prime examples are  
51 radiation therapy treatment planning and tomographic reconstruction, but there are others  
52 such as image registration. Some well-cited classical publications on the topic are<sup>1-12</sup> and  
53 some recent articles are<sup>13-26</sup>.

54 In a typical medical physics application, one uses *constrained optimization*, where the  
55 constraints come from the desire to produce a solution that is *constraints-compatible*, in  
56 the sense of meeting the requirements provided by physically or otherwise obtained con-  
57 straints. In radiation therapy treatment planning, the requirements are usually in the form

58 of constraints prescribed by the treatment planner on the doses to be delivered at specific  
59 locations in the body. These doses in turn depend on information provided by an imaging  
60 instrument, typically a Magnetic Resonance Imaging (MRI) or a Computerized Tomogra-  
61 phy (CT) scanner. In tomography, the constraints come from the detector readings of the  
62 instrument. In such applications, it is typically the case that a large number of solutions  
63 would be considered good enough from the point of view of being constraints-compatible;  
64 to a large extent, but not entirely, due to the fact that there is uncertainty as to the exact  
65 nature of the constraints (for example, due to noise in the data collection). In such a case,  
66 an optimization criterion is introduced that helps us to distinguish the “better” constraints-  
67 compatible solutions (for example, this criterion could be the total dose to be delivered to  
68 the body, which may vary quite a bit between radiation therapy treatment plans that are  
69 compatible with the constraints on the doses delivered to individual locations).

70 The superiorization methodology (see, for example,<sup>22,27-32</sup>) is a recently-developed heuris-  
71 tic approach to optimization. The word *heuristic* is used here in the sense that the process  
72 is not guaranteed to lead to an optimum according to the given criterion; approaches aimed  
73 at processes that are guaranteed in that sense are usually referred to as *exact*. Heuristic  
74 approaches have been found useful in practical applications of optimization, mainly because  
75 they are often computationally much less expensive than their exact counterparts, but nev-  
76 ertheless provide solutions that are appropriate for the application at hand<sup>33-35</sup>.

77 The underlying idea of the superiorization approach is the following. In many applica-  
78 tions there exists a computationally-efficient iterative algorithm that produces a constraints-  
79 compatible solution for the given constraints. (An example of this for radiation therapy  
80 treatment planning is reported in<sup>36</sup>, its clinical use is discussed in<sup>15</sup>.) Furthermore, often  
81 the algorithm is *perturbation resilient* in the sense that, even if certain kinds of changes are  
82 made at the end of each iterative step, the algorithm still produces a constraints-compatible  
83 solution<sup>27-30</sup>. This property is exploited in the superiorization approach by using such per-  
84 turbations to steer the algorithm to a solution that is not only constraints-compatible, but is  
85 also desirable according to a specified optimization criterion. The approach is very general,  
86 it is applicable to many iterative procedures and optimization criteria.

87 The current paper presents a major advance in the practice and theory of superiorization.  
88 The previous publications<sup>22,27-32</sup> used the intuitive idea to present some superiorization  
89 algorithms, in this paper the reader will find a totally automatic procedure that turns an

90 iterative algorithm into its superiorized version. This version will produce an output that  
91 is as constraints-compatible as the output of the original algorithm, but it is superior to  
92 that according to an optimization criterion. This claim is mathematically shown to be  
93 true for a very large class of iterative algorithms and for optimization criteria in general,  
94 typical restrictions (such as convexity) on the optimization criterion are not essential for  
95 the material presented below. In order to make precise and validate this broad claim, we  
96 present here a new theoretical framework. The framework of<sup>29</sup> is a precursor of what we  
97 present here, but it is a restricted one, since it assumes that the constraints can be all  
98 satisfied simultaneously, which is often false in medical physics applications. There is no  
99 such restriction in the presentation below.

100 The idea of designing algorithms that use interlacing steps of two different kinds (in our  
101 case, one kind of steps aim at constraints-compatibility and the other kind of steps aim at  
102 improvement of the optimization criterion) is well-established and, in fact, is made use of  
103 in many approaches that have been proposed with exact constrained optimization in mind;  
104 see, for example, the works of Helou Neto and De Pierro<sup>37,38</sup>, of Nurminski<sup>39</sup>, of Combettes  
105 and coworkers<sup>40,41</sup>, of Sidky and Pan and coworkers<sup>23,42,43</sup> and of Defrise and coworkers<sup>44</sup>.  
106 However, none of these approaches can do what can be done by the superiorization approach  
107 as presented below, namely the automatic production of a heuristic constrained optimization  
108 algorithm from an iterative algorithm for constraints-compatibility. For example, in<sup>37</sup> it is  
109 assumed (just as in the theory presented in our<sup>29</sup>) that all the constraints can be satisfied  
110 simultaneously.

111 A major motivator for the additional theory presented in the current paper is to get rid  
112 of this assumption, which is not reasonable when handling real problems of medical physics.  
113 Motivated by similar considerations, Helou Neto and De Pierro<sup>38</sup> present an alternative  
114 approach that does not require this unreasonable assumption. However, in order to solve  
115 such a problem, they end up with iterative algorithms of a particular form rather than having  
116 the generality of being able to turn any constraints-compatibility seeking algorithm into a  
117 superiorized one capable of handling constrained optimization. Also, the assumptions they  
118 have to make in order to prove their convergence result (their Theorem 15) indicate that  
119 their approach is applicable to a smaller class of constrained optimization problems than  
120 the superiorization approach whose applicability seems to be more general. However, for  
121 the mathematical purist, we point out that they present an exact constrained optimization

122 algorithm, while superiorization is a heuristic approach. Whether this is relevant to medical  
123 physics practice is not clear: exact algorithms are not run forever, but are stopped according  
124 to some stopping-rule, the relevant questions in comparing two algorithms are the quality  
125 of the actual output and the computation time needed to obtain it.

126 Ultimately, the quality of the outputs should be evaluated by some figures of merit  
127 relevant to the medical task at hand. An example of a careful study of this kind that  
128 involves superiorization is in<sup>30</sup> (Section 4.3), which reports on comparing in CT the efficacy  
129 of constrained optimization reconstruction algorithms for the detection of low-contrast brain  
130 tumors by using the method of statistical hypothesis testing (which provides a P-value that  
131 indicates the significance by which we can reject the null hypothesis that the two algorithms  
132 are equally efficacious in favor of the alternative that one is preferable). Such studies bundle  
133 together two things: (i) the formulation of the constrained optimization task and (ii) the  
134 performance of the algorithm in performing that task. The first of these requires a translation  
135 of the medical aim into a mathematical model, it is important that this model should be  
136 appropriately chosen.

137 The superiorization approach is not about choosing this model, it kicks in once the model  
138 is chosen and aims at producing an output that is “good” according to the mathematical  
139 specifications of the constraints and of the optimization criterion. Thus superiorization has  
140 been used to compare the effects on the quality of the output in CT when the optimization  
141 criterion is specified by total variation (TV) versus by entropy<sup>28</sup> or versus by the  $\ell_1$ -norm  
142 of the Haar transform<sup>32</sup>. However, the current paper is not about discussing how to trans-  
143 late the underlying medical physics task into a constrained optimization problem. For our  
144 purposes here, we are assuming that the mathematical model has been worked out and  
145 concentrate on the algorithmic approach for solving the resulting constrained optimization  
146 problem. We claim that the evaluation of such algorithms should not be based on the  
147 medical figures of merit mentioned at the beginning of the previous paragraph, but rather  
148 on their performance in solving the mathematical problem. If “good” solutions to the con-  
149 strained optimization problem are not medically efficacious, that indicates that something is  
150 wrong with the mathematical model and not that something is wrong with the algorithmic  
151 approach. For this reason, in this paper we will not carry out a careful investigation of the  
152 medical efficacy of any algorithm in the manner that we have done in<sup>30</sup> (Section 4.3), but will  
153 restrict ourselves to a simple illustration of the performance of the superiorization approach

154 as compared to the previously published algorithm of<sup>42</sup> that is aimed at performing exact  
155 minimization.

156 Examples of such studies already exist. Superiorization was compared in<sup>27</sup> with Algorithm  
157 6 of<sup>40</sup> and in<sup>45</sup> with the algorithm of Goldstein and Osher that they refer to as TwIST<sup>46</sup> with  
158 split Bregman<sup>47</sup> as the substep. In both cases the implementation was done by the proposers  
159 of the algorithms. In these reported instances superiorization did well: the constraints-  
160 compatibility and the value of the function to be minimized were very similar for the outputs  
161 produced by the algorithms being compared, but the superiorization algorithm produced its  
162 output four times faster than the alternative. It would be unjustified to draw any general  
163 conclusions on the mathematical performance and speed of superiorization based on just a  
164 few experiments, but the reported results are encouraging.

165 However, the main reason why we advocate superiorization is different from what is  
166 discussed above. The reason why we claim it to be helpful in medical physics research is  
167 that it has the potential of saving a lot of time and effort for the researcher. Let us consider  
168 a historical example. Likelihood optimization using the iterative process of expectation  
169 maximization (EM)<sup>48</sup> gained immediate and wide acceptance in the emission tomography  
170 community. It was observed that irregular high amplitude patterns occurred in the image  
171 with a large number of iterations, but it was not until five years later that this problem  
172 was corrected<sup>49</sup> by the use of a maximum a posteriority probability (MAP) algorithm with  
173 a multivariate Gaussian prior. Had we had at our disposal the superiorization approach,  
174 then the introduction of an optimization criterion (Gaussian or other) into the iterative  
175 expectation maximization (EM) process would have been a simple matter and we would  
176 have saved the time and effort spent on designing a special purpose algorithm for the MAP  
177 formulation. A *TV*-superiorization of the EM algorithm is presented in<sup>50</sup>.

178 Even though our major claim for superiorization is that it provides a quick route to  
179 algorithms for the practical solution of constrained optimization problems, before leaving  
180 this introduction let us bring up a question that has to do with the performance of the  
181 resulting algorithms: Will superiorization produce superior results to those produced by  
182 contemporary MAP methods or is it faster than the better of such methods? At this stage  
183 we have not yet developed the mathematical notation to discuss this question in a rigorous  
184 manner, we return to it in Subsection **II F**.

185 In the next section we present in detail the superiorization methodology. In the subse-

186 quent section we provide an illustrative example by reporting on reconstructions produced  
 187 by algorithms applied to simulated computerized tomography data of a head cross-section.  
 188 In the final section we discuss our results and present our conclusions.

## 189 II. THE SUPERIORIZATION METHODOLOGY

### 190 A. Problem sets, proximity functions and $\varepsilon$ -compatibility

191 Although optimization is often studied in a more general context (such as in Hilbert or  
 192 Banach spaces), in medical physics we usually deal with a special case, where optimization  
 193 is performed in a *Euclidean space*  $\mathbb{R}^J$  (the space of  $J$ -dimensional vectors of real numbers,  
 194 where  $J$  is a positive integer). As often appropriate in practice, we further restrict the  
 195 domain of optimization to a nonempty subset  $\Omega$  of  $\mathbb{R}^J$  (such as the *nonnegative orthant*  $\mathbb{R}_+^J$   
 196 that consists of vectors all of whose components are nonnegative).

197 We now turn to formalizing the notion of being compatible with given constraints, a  
 198 notion that we have used informally in the previous section. In any application, there is a  
 199 *problem set*  $\mathbb{T}$ ; each *problem*  $T \in \mathbb{T}$  is essentially a description of the constraints in that  
 200 particular case. For example, for a tomographic scanner, the problem of reconstruction for  
 201 a particular patient at a particular time is determined by the measurements taken by the  
 202 scanner for that patient at that time. The intuitive notion of constraints-compatibility is  
 203 formalized by the use of a *proximity function*  $\mathcal{P}r$  on  $\mathbb{T}$  such that, for every  $T \in \mathbb{T}$ ,  $\mathcal{P}r_T$   
 204 maps  $\Omega$  into  $\mathbb{R}_+$ , the set of nonnegative real numbers; i.e.,  $\mathcal{P}r_T : \Omega \rightarrow \mathbb{R}_+$ . Intuitively we  
 205 think of  $\mathcal{P}r_T(\mathbf{x})$  as an indicator of how incompatible  $\mathbf{x}$  is with the constraints of  $T$ . For  
 206 example, in tomography,  $\mathcal{P}r_T(\mathbf{x})$  should indicate by how much a proposed reconstruction  
 207 that is described by an  $\mathbf{x}$  in  $\Omega$  violates the constraints of the problem  $T$  that are provided  
 208 by the measurements taken by the scanner. For example, if we use  $\mathbf{b}$  to denote the vector  
 209 of estimated line integrals based on the measurements obtained by the scanner and by  $\mathbf{A}$   
 210 the system matrix of the scanner, then a possible choice for the proximity function is the  
 211 norm-distance  $\|\mathbf{b} - \mathbf{A}\mathbf{x}\|$ , which we will use as an example in the discussions that follow.  
 212 An alternative legitimate choice for the proximity function is the Kullback-Leibler distance  
 213  $KL(\mathbf{b}, \mathbf{A}\mathbf{x})$ , which is the negative log-likelihood of a statistical model in tomography. The  
 214 special case  $\mathcal{P}r_T(\mathbf{x}) = 0$  is interpreted by saying that  $\mathbf{x}$  is perfectly compatible with the

215 constraints; due to the presence of noise in practical applications, it is quite conceivable  
 216 that there is no  $\mathbf{x}$  that is perfectly compatible with the constraints, and we accept an  $\mathbf{x}$   
 217 as constraints-compatible as long as the value of  $\mathcal{P}r_T(\mathbf{x})$  is considered to be small enough  
 218 to justify that decision. Combining these two concepts leads to the notion of a *problem*  
 219 *structure*, which is a pair  $\langle \mathbb{T}, \mathcal{P}r \rangle$ , where  $\mathbb{T}$  is a nonempty problem set and  $\mathcal{P}r$  is a proximity  
 220 function on  $\mathbb{T}$ . For a problem structure  $\langle \mathbb{T}, \mathcal{P}r \rangle$ , a problem  $T \in \mathbb{T}$ , a nonnegative  $\varepsilon$  and an  
 221  $\mathbf{x} \in \Omega$ , we say that  $\mathbf{x}$  is  $\varepsilon$ -compatible with  $T$  provided that  $\mathcal{P}r_T(\mathbf{x}) \leq \varepsilon$ .

222 As an example (whose applicability to tomographic reconstruction is illustrated in Section  
 223 III), consider the problem structure that arises from the desire to find nonnegative solutions  
 224 of sequences of blocks of linear equations. Then the appropriate choices are  $\Omega = \mathbb{R}_+^J$  and  
 225 the problem structure is  $\langle \mathbb{S}, Res \rangle$ , where the problem set  $\mathbb{S}$  is

$$\begin{aligned} \mathbb{S} = & \{ \{ (\mathbf{a}^1, b_1), \dots, (\mathbf{a}^{\ell_1}, b_{\ell_1}) \}, \dots, \\ & \{ (\mathbf{a}^{\ell_1+\dots+\ell_{W-1}+1}, b_{\ell_1+\dots+\ell_{W-1}+1}), \dots, (\mathbf{a}^{\ell_1+\dots+\ell_W}, b_{\ell_1+\dots+\ell_W}) \} \} | \\ & W \text{ is a positive integer and,} \\ & \text{for } 1 \leq w \leq W, \ell_w \text{ is a positive integer and,} \\ & \text{for } 1 \leq i \leq \ell_1 + \dots + \ell_W, \mathbf{a}^i \in \mathbb{R}^J \text{ and } b_i \in \mathbb{R} \} \end{aligned} \quad (1)$$

226 and the proximity function  $Res$  on  $\mathbb{S}$  is defined, for any problem  $S = (\{(\mathbf{a}^1, b_1),$   
 227  $\dots, (\mathbf{a}^{\ell_1}, b_{\ell_1})\}, \dots, \{(\mathbf{a}^{\ell_1+\dots+\ell_{W-1}+1}, b_{\ell_1+\dots+\ell_{W-1}+1}), \dots, (\mathbf{a}^{\ell_1+\dots+\ell_W}, b_{\ell_1+\dots+\ell_W})\})$  in  $\mathbb{S}$  and  
 228 for any  $\mathbf{x} \in \Omega$ , by

$$Res_S(\mathbf{x}) = \sqrt{\sum_{i=1}^{\ell_1+\dots+\ell_W} (b_i - \langle \mathbf{a}^i, \mathbf{x} \rangle)^2}. \quad (2)$$

229 Note that each element of this problem set  $\mathbb{S}$  specifies an ordered sequence of  $W$  blocks  
 230 of linear equations of the form  $\langle \mathbf{a}^i, \mathbf{x} \rangle = b_i$  where  $\langle *, * \rangle$  denotes the inner product in  $\mathbb{R}^J$   
 231 (and thus  $\mathbb{S}$  is an appropriate representation of the so-called “ordered subsets” approach to  
 232 tomographic reconstruction<sup>51</sup>, as well as of other earlier-published block-iterative methods  
 233 that proposed essentially the same idea<sup>52–54</sup>). The proximity function  $Res$  on  $\mathbb{S}$  is the *residual*  
 234 that we get when a particular  $\mathbf{x}$  is substituted into all the equations of a particular problem  
 235  $S$ .



236

## B. Algorithms and outputs

237 We now define the concept of an algorithm in the general context of problem structures.  
 238 For technical reasons that will become clear as we proceed with our development, we intro-  
 239 duce an additional set  $\Delta$ , such that  $\Omega \subseteq \Delta \subseteq \mathbb{R}^J$ . (Both  $\Omega$  and  $\Delta$  are assumed to be known  
 240 and fixed for any particular problem structure  $\langle \mathbb{T}, \mathcal{P}r \rangle$ .) An *algorithm*  $\mathbf{P}$  for a problem  
 241 structure  $\langle \mathbb{T}, \mathcal{P}r \rangle$  assigns to each problem  $T \in \mathbb{T}$  an operator  $\mathbf{P}_T : \Delta \rightarrow \Omega$ . This definition is  
 242 used to define iterative processes that, for any *initial point*  $\mathbf{x} \in \Omega$ , produce the (potentially)  
 243 infinite sequence  $\left( (\mathbf{P}_T)^k \mathbf{x} \right)_{k=0}^{\infty}$  (that is, the sequence  $\mathbf{x}, \mathbf{P}_T \mathbf{x}, \mathbf{P}_T (\mathbf{P}_T \mathbf{x}), \dots$ ) of points in  
 244  $\Omega$ . We discuss below how such a potentially infinite process is terminated in practice.

245 Selecting  $\Omega = \mathbb{R}_+^J$  and  $\Delta = \mathbb{R}^J$  for the problem structure  $\langle \mathbb{S}, Res \rangle$  of the previous subsec-  
 246 tion, an example of an algorithm  $\mathbf{R}$  is specified by

$$\mathbf{R}_S \mathbf{x} = \mathbf{Q} \mathbf{B}_{S_W} \cdots \mathbf{B}_{S_1} \mathbf{x}, \quad (3)$$

247 where  $S$  is the problem specified above (2) and, for  $1 \leq w \leq W$ ,  $\mathbf{B}_{S_w} : \Delta \rightarrow \Delta$  is defined by

$$\mathbf{B}_{S_w} \mathbf{x} = \mathbf{x} + \frac{1}{\ell_w} \sum_{i=\ell_1+\dots+\ell_{w-1}+1}^{\ell_1+\dots+\ell_w} \frac{b_i - \langle \mathbf{a}^i, \mathbf{x} \rangle}{\|\mathbf{a}^i\|^2} \mathbf{a}^i, \quad (4)$$

248 where  $\|\mathbf{a}\|$  denotes the norm of the vector  $\mathbf{a}$  in  $\mathbb{R}^J$ , and  $\mathbf{Q} : \Delta \rightarrow \Omega$  is defined by

$$(\mathbf{Q}\mathbf{x})_j = \max \{0, \mathbf{x}_j\}, \quad \text{for } 1 \leq j \leq J. \quad (5)$$

249 Note that  $\mathbf{R}_S : \Delta \rightarrow \Omega$ . This specific algorithm  $\mathbf{R}$  is a typical example of the so-called block-  
 250 iterative methods mentioned above. Except for the presence of  $\mathbf{Q}$  in (3), which enforces  
 251 nonnegativity of the components, it is identical to an algorithm used and illustrated in<sup>31</sup>.  
 252 With the  $\mathbf{Q}$  absent from the definition of the algorithm,  $\Omega$  has to be the whole of  $\mathbb{R}^J$ ; the  
 253 practical consequence of the presence versus the absence of  $\mathbf{Q}$  in the tomographic application  
 254 is illustrated in Subsection III D. We note also that special cases of the presented algorithm  
 255 include the classical reconstruction methods ART (if  $\ell_w = 1$ , for  $1 \leq w \leq W$ ) and SIRT (if  
 256  $W = 1$ ); see, for example, Chapters 11 and 12 of<sup>55</sup>.

257 For a problem structure  $\langle \mathbb{T}, \mathcal{P}r \rangle$ , a  $T \in \mathbb{T}$ , an  $\varepsilon \in \mathbb{R}_+$  and a sequence  $R = (\mathbf{x}^k)_{k=0}^{\infty}$   
 258 of points in  $\Omega$ , we use  $O(T, \varepsilon, R)$  to denote the  $\mathbf{x} \in \Omega$  that has the following properties:  
 259  $\mathcal{P}r_T(\mathbf{x}) \leq \varepsilon$  and there is a nonnegative integer  $K$  such that  $\mathbf{x}^K = \mathbf{x}$  and, for all nonnegative  
 260 integers  $k < K$ ,  $\mathcal{P}r_T(\mathbf{x}^k) > \varepsilon$ . Clearly, if there is such an  $\mathbf{x}$ , then it is unique. If there is no

261 such  $\mathbf{x}$ , then we say that  $O(T, \varepsilon, R)$  is *undefined*, otherwise we say that it is *defined*. The  
 262 intuition behind this definition is the following: if we think of  $R$  as the (infinite) sequence of  
 263 points that is produced by an algorithm (intended for the problem  $T$ ) without a termination  
 264 criterion, then  $O(T, \varepsilon, R)$  is the *output* produced by that algorithm when we add to it  
 265 instructions that make it terminate as soon as it reaches a point that is  $\varepsilon$ -compatible with  
 266  $T$ .

### 267 C. Bounded perturbation resilience

268 The notion of a *bounded perturbations resilient* algorithm  $\mathbf{P}$  for a problem structure  
 269  $\langle \mathbb{T}, \mathcal{P}r \rangle$  has been defined in a mathematically precise manner<sup>29</sup>. However, that definition  
 270 is not satisfactory from the point of view of applications in medical physics (or indeed in  
 271 any area involving noisy data), because it is useful only for problems  $T$  for which there is  
 272 a perfectly compatible solution (that is, an  $\mathbf{x}$  such that  $\mathcal{P}r_T(\mathbf{x}) = 0$ ). We therefore extend  
 273 here that notion as follows. An algorithm  $\mathbf{P}$  for a problem structure  $\langle \mathbb{T}, \mathcal{P}r \rangle$  is said to be  
 274 *strongly perturbation resilient* if, for all  $T \in \mathbb{T}$ ,

- 275 (i) there exists an  $\varepsilon \in \mathbb{R}_+$  such that  $O\left(T, \varepsilon, \left((\mathbf{P}_T)^k \mathbf{x}\right)_{k=0}^{\infty}\right)$  is defined for every  $\mathbf{x} \in \Omega$ ;  
 276 (ii) for all  $\varepsilon \in \mathbb{R}_+$  such that  $O\left(T, \varepsilon, \left((\mathbf{P}_T)^k \mathbf{x}\right)_{k=0}^{\infty}\right)$  is defined for every  $\mathbf{x} \in \Omega$ , we also  
 277 have that  $O(T, \varepsilon', R)$  is defined for every  $\varepsilon' > \varepsilon$  and for every sequence  $R = (\mathbf{x}^k)_{k=0}^{\infty}$   
 278 of points in  $\Omega$  generated by

$$\mathbf{x}^{k+1} = \mathbf{P}_T(\mathbf{x}^k + \beta_k \mathbf{v}^k), \text{ for all } k \geq 0, \quad (6)$$

279 where  $\beta_k \mathbf{v}^k$  are *bounded perturbations*, meaning that the sequence  $(\beta_k)_{k=0}^{\infty}$  of nonnega-  
 280 tive real numbers is *summable* (that is,  $\sum_{k=0}^{\infty} \beta_k < \infty$ ), the sequence  $(\mathbf{v}^k)_{k=0}^{\infty}$  of vectors  
 281 in  $\mathbb{R}^J$  is bounded and, for all  $k \geq 0$ ,  $\mathbf{x}^k + \beta_k \mathbf{v}^k \in \Delta$ .

282 In less formal terms, the second of these properties says that for a strongly perturbation  
 283 resilient algorithm we have that, for every problem and any nonnegative real number  $\varepsilon$ , if it  
 284 is the case that for all initial points from  $\Omega$  the infinite sequence produced by the algorithm  
 285 contains an  $\varepsilon$ -compatible point, then it will also be the case that all perturbed sequences  
 286 satisfying (6) contain an  $\varepsilon'$ -compatible point, for any  $\varepsilon' > \varepsilon$ .

287 Having defined the notion of a strongly perturbation resilient algorithm, we next show  
 288 that this notion is of relevance to problems in medical physics. We illustrate the use of this  
 289 in tomography in the next section. We first need to introduce some mathematical concepts.

290 Given an algorithm  $\mathbf{P}$  for a problem structure  $\langle \mathbb{T}, \mathcal{Pr} \rangle$  and a  $T \in \mathbb{T}$ , we say that  
 291  $\mathbf{P}$  is *convergent for  $T$*  if, for every  $\mathbf{x} \in \Omega$ , there exists a unique  $\mathbf{y}(\mathbf{x}) \in \Omega$  such that,  
 292  $\lim_{k \rightarrow \infty} (\mathbf{P}_T)^k \mathbf{x} = \mathbf{y}(\mathbf{x})$ , meaning that for every positive real number  $\delta$ , there exist a non-  
 293 negative integer  $K$ , such that  $\|(\mathbf{P}_T)^k \mathbf{x} - \mathbf{y}(\mathbf{x})\| \leq \delta$ , for all nonnegative integers  $k \geq K$ .  
 294 If, in addition, there exists a  $\gamma \in \mathbb{R}_+$  such that  $\mathcal{Pr}_T(\mathbf{y}(\mathbf{x})) \leq \gamma$ , for every  $\mathbf{x} \in \Omega$ , then we  
 295 say that  $\mathbf{P}$  is *boundedly convergent for  $T$* .

296 A function  $f : \Omega \rightarrow \mathbb{R}$  is *uniformly continuous* if, for every  $\varepsilon > 0$  there exists a  $\delta > 0$ ,  
 297 such that, for all  $\mathbf{x}, \mathbf{y} \in \Omega$ ,  $|f(\mathbf{x}) - f(\mathbf{y})| \leq \varepsilon$  provided that  $\|\mathbf{x} - \mathbf{y}\| \leq \delta$ . An example of a  
 298 uniformly continuous function is  $Res_S$  of (2), for any  $S \in \mathbb{S}$ . This can be proved by observing  
 299 that the right-hand side of (2) can be rewritten in vector/matrix form as  $\|\mathbf{b} - \mathbf{A}\mathbf{x}\|$  and  
 300 then selecting, for any given  $\varepsilon > 0$ ,  $\delta$  to be  $\varepsilon / \|\mathbf{A}\|$ , where  $\|\mathbf{A}\|$  denotes the matrix norm of  
 301  $\mathbf{A}$ .

302 An operator  $\mathbf{O} : \Delta \rightarrow \Omega$ , is *nonexpansive* if  $\|\mathbf{O}\mathbf{x} - \mathbf{O}\mathbf{y}\| \leq \|\mathbf{x} - \mathbf{y}\|$ , for all  $\mathbf{x}, \mathbf{y} \in \Delta$ .  
 303 An example of a nonexpansive operator is the  $\mathbf{R}_S$  of (3). The proof of this is also simple.  
 304 It follows from discussions regarding similar claims in<sup>27</sup> that the  $\mathbf{B}_{S_w} : \mathbb{R}^J \rightarrow \mathbb{R}^J$  of (4) is a  
 305 nonexpansive operator, for  $1 \leq w \leq W$ , and that the operator  $\mathbf{Q}$  of (5) is also nonexpansive.  
 306 Obviously, a sequential application of nonexpansive operators results in a nonexpansive  
 307 operator and thus  $\mathbf{R}_S$  is nonexpansive.

308 Now we state an important new result that gives sufficient conditions for strong perturba-  
 309 tion resilience: If  $\mathbf{P}$  is an algorithm for a problem structure  $\langle \mathbb{T}, \mathcal{Pr} \rangle$  such that,  
 310 for all  $T \in \mathbb{T}$ ,  $\mathbf{P}$  is boundedly convergent for  $T$ ,  $\mathcal{Pr}_T : \Omega \rightarrow \mathbb{R}$  is uniformly  
 311 continuous and  $\mathbf{P}_T : \Delta \rightarrow \Omega$  is nonexpansive, then  $\mathbf{P}$  is strongly perturbation  
 312 resilient. The importance of this result lies in the fact that the rather ordinary condition  
 313 of uniform continuity for the proximity function and the reasonable conditions of bounded  
 314 convergence and nonexpansiveness of the algorithmic operators guarantee that we end up  
 315 with a strongly perturbation resilient algorithm. The proof of this new result involves some  
 316 mathematical technicalities and is therefore presented in the Appendix as Theorem 1.

317

### D. Optimization criterion and nonascending vector

318 Now suppose, as is indeed the case for the constrained optimization problems discussed  
 319 in the previous section, that in addition to a problem structure  $\langle \mathbb{T}, \mathcal{Pr} \rangle$  we are also provided  
 320 with an optimization criterion, which is specified by a function  $\phi : \Delta \rightarrow \mathbb{R}$ , with the  
 321 convention that a point in  $\Delta$  for which the value of  $\phi$  is smaller is considered *superior* (from  
 322 the point of view of our application) to a point in  $\Delta$  for which the value of  $\phi$  is larger. In the  
 323 tomography context, any of the functions of  $\mathbf{x}$  that are listed as a “secondary optimization  
 324 criterion” (an alternative name is a “regularizer”) in Section 6.4 of<sup>55</sup> is an acceptable choice  
 325 for the optimization criterion  $\phi$ . These include weighted norms, the negative of Shannon’s  
 326 entropy and total variation. It is the last of these that we discuss in detail in the illustrative  
 327 example below. The essential idea of the *superiorization methodology* presented in this paper  
 328 is to make use of the perturbations of (6) to transform a strongly perturbation resilient  
 329 algorithm that seeks a constraints-compatible solution into one whose outputs are equally  
 330 good from the point of view of constraints-compatibility, but are superior according to the  
 331 optimization criterion. We do this by producing from the algorithm another one, called its  
 332 *superiorized* version, by making sure not only that the  $\beta_k \mathbf{v}^k$  are bounded perturbations, but  
 333 also that  $\phi(\mathbf{x}^k + \beta_k \mathbf{v}^k) \leq \phi(\mathbf{x}^k)$ , for all  $k \geq 0$ .

334 In order to ensure this we introduce a new concept (closely related to the concept of a  
 335 “descent direction” that is widely used in optimization). Given a function  $\phi : \Delta \rightarrow \mathbb{R}$  and a  
 336 point  $\mathbf{x} \in \Delta$ , we say that a vector  $\mathbf{d} \in \mathbb{R}^J$  is *nonascending* for  $\phi$  at  $\mathbf{x}$  if  $\|\mathbf{d}\| \leq 1$  and

$$\begin{aligned} &\text{there is a } \delta > 0 \text{ such that for all } \lambda \in [0, \delta], \\ &(\mathbf{x} + \lambda \mathbf{d}) \in \Delta \text{ and } \phi(\mathbf{x} + \lambda \mathbf{d}) \leq \phi(\mathbf{x}). \end{aligned} \tag{7}$$

337 Note that irrespective of the choices of  $\phi$  and  $\mathbf{x}$ , there is always at least one nonascending  
 338 vector  $\mathbf{d}$  for  $\phi$  at  $\mathbf{x}$ , namely the zero-vector, all of whose components are zero. This is a useful  
 339 fact for proving results concerning the guaranteed behavior of our proposed procedures.  
 340 However, in order to steer our algorithms toward a point at which the value of  $\phi$  is small,  
 341 we need to find a  $\mathbf{d}$  such that  $\phi(\mathbf{x} + \lambda \mathbf{d}) < \phi(\mathbf{x})$  rather than just  $\phi(\mathbf{x} + \lambda \mathbf{d}) \leq \phi(\mathbf{x})$  as in  
 342 (7). In some earlier papers on superiorization<sup>27-31</sup> it was assumed that  $\Delta = \mathbb{R}^J$  and that  $\phi$   
 343 is a convex function. This implied that, for any point  $\mathbf{x} \in \Delta$ ,  $\phi$  had a subgradient  $\mathbf{g} \in \mathbb{R}^J$  at  
 344 the point  $\mathbf{x}$ . It was suggested that if there is such a  $\mathbf{g}$  with a positive norm, then  $\mathbf{d}$  should  
 345 be chosen to be  $-\mathbf{g}/\|\mathbf{g}\|$ , otherwise  $\mathbf{d}$  should be chosen to be the zero vector. However,

346 there are approaches (not involving subgradients) to selecting an appropriate  $\mathbf{d}$ ; an example  
 347 can be found in<sup>32</sup> in which  $\mathbf{d}$  is found without using subgradients for the case when  $\phi$  is the  
 348  $\ell_1$ -norm of the Haar transform. The method we used for selecting a nonascending vector in  
 349 the experiments reported in this paper is specified at the end of Subsection III A.

### 350 E. Superiorized version of an algorithm

351 We now make precise the ingredients needed for transforming an algorithm into its su-  
 352 periorized version. Let  $\Omega$  and  $\Delta$  be the underlying sets for a problem structure  $\langle \mathbb{T}, \mathcal{P}r \rangle$   
 353 ( $\Omega \subseteq \Delta \subseteq \mathbb{R}^J$ , as discussed at the beginning of Subsection II B),  $\mathbf{P}$  be an algorithm for  
 354  $\langle \mathbb{T}, \mathcal{P}r \rangle$  and  $\phi : \Delta \rightarrow \mathbb{R}$ . The following description of the Superiorized Version of Algorithm  
 355  $\mathbf{P}$  produces, for any problem  $T \in \mathbb{T}$ , a sequence  $R_T = (\mathbf{x}^k)_{k=0}^\infty$  of points in  $\Omega$  for which, for  
 356 all  $k \geq 0$ , (6) is satisfied. We show this to be true, for any algorithm  $\mathbf{P}$ , after the description  
 357 of the Superiorized Version of Algorithm  $\mathbf{P}$ . Furthermore, since the sequence  $R_T$  is steered  
 358 by Superiorized Version of Algorithm  $\mathbf{P}$  toward a reduced value of  $\phi$ , there is an intuitive  
 359 expectation that the output of the superiorized version is likely to be superior (from the  
 360 point of view of the optimization criterion  $\phi$ ) to the output of the original unperturbed  
 361 algorithm. This last statement is not precise and so it cannot be proved in a mathematical  
 362 sense for an arbitrary algorithm  $\mathbf{P}$ ; however, that should not stop us from applying the  
 363 easy procedure given below for automatically producing the Superiorized Version of  $\mathbf{P}$  and  
 364 experimentally checking whether it indeed provides us with outputs superior to those of the  
 365 original algorithm. The well-demonstrated nature of heuristic optimization approaches is  
 366 that they often work in practice even when their performance cannot be guaranteed to be  
 367 optimal<sup>33–35</sup>.

368 Nevertheless, we can push our theory further than the hope expressed in the last para-  
 369 graph, by considering superiorized versions of algorithms that satisfy some condition. In  
 370 this paper, the condition that we discuss is strong perturbation resilience. We show below  
 371 that if  $\mathbf{P}$  is strongly perturbation resilient, then, for any problem  $T \in \mathbb{T}$ , a sequence  $R_T$   
 372 produced by its superiorized version has the following desirable property: For all  $\varepsilon \in \mathbb{R}_+$ , if  
 373  $O(T, \varepsilon, ((\mathbf{P}_T)^k \mathbf{x})_{k=0}^\infty)$  is defined for every  $\mathbf{x} \in \Omega$ , then  $O(T, \varepsilon', R_T)$  is also defined for every  
 374  $\varepsilon' > \varepsilon$ ; in other words, the Superiorized Version of Algorithm  $\mathbf{P}$  provides an  $\varepsilon'$ -compatible  
 375 output. As stated above, the advantage of the superiorized version is that its output is

376 likely to be superior to the output of the original unperturbed algorithm. We point out that  
 377 strong perturbation resilience is a sufficient, but not necessary, condition for guaranteeing  
 378 such desirable behavior of the superiorized version, finding additional sufficient conditions  
 379 and proving that algorithms that we wish to superiorize satisfy such conditions is part of  
 380 our ongoing research.

381 The superiorized version assumes that we have available a summable sequence  $(\gamma_\ell)_{\ell=0}^\infty$  of  
 382 positive real numbers (for example,  $\gamma_\ell = a^\ell$ , where  $0 < a < 1$ ) and it generates, simultane-  
 383 ously with the sequence  $(\mathbf{x}^k)_{k=0}^\infty$ , sequences  $(\mathbf{v}^k)_{k=0}^\infty$  and  $(\beta_k)_{k=0}^\infty$ . The latter is generated as  
 384 a subsequence of  $(\gamma_\ell)_{\ell=0}^\infty$ , resulting in a summable sequence  $(\beta_k)_{k=0}^\infty$ . The algorithm further  
 385 depends on a specified initial point  $\bar{\mathbf{x}} \in \Omega$  and on a positive integer  $N$ . It makes use of a  
 386 logical variable called *loop*.

### 387 Superiorized Version of Algorithm P

388 (i) set  $k = 0$

389 (ii) set  $\mathbf{x}^k = \bar{\mathbf{x}}$

390 (iii) set  $\ell = -1$

391 (iv) repeat

392 (v) set  $n = 0$

393 (vi) set  $\mathbf{x}^{k,n} = \mathbf{x}^k$

394 (vii) while  $n < N$

395 (viii) set  $\mathbf{v}^{k,n}$  to be a nonascending vector for  $\phi$  at  $\mathbf{x}^{k,n}$

396 (ix) set  $loop = true$

397 (x) while  $loop$

398 (xi) set  $\ell = \ell + 1$

399 (xii) set  $\beta_{k,n} = \gamma_\ell$

400 (xiii) set  $\mathbf{z} = \mathbf{x}^{k,n} + \beta_{k,n} \mathbf{v}^{k,n}$

401 (xiv) if  $\mathbf{z} \in \Delta$  and  $\phi(\mathbf{z}) \leq \phi(\mathbf{x}^k)$  then

402 (xv)                                    **set**  $n = n + 1$

403 (xvi)                                   **set**  $\mathbf{x}^{k,n} = \mathbf{z}$

404 (xvii)                                **set**  $loop = false$

405 (xviii)                            **set**  $\mathbf{x}^{k+1} = \mathbf{P}_T \mathbf{x}^{k,N}$

406 (xix)                                **set**  $k = k + 1$

407 Next we analyze the behavior of the Superiorized Version of Algorithm **P**.

408     The iteration number  $k$  is set to 0 in (i) and  $\mathbf{x}^k = \mathbf{x}^0$  is set to its initial value  $\bar{\mathbf{x}}$  in (ii). The  
409 integer index  $\ell$  for picking the next element from the sequence  $(\gamma_\ell)_{\ell=0}^\infty$  is initialized to  $-1$  by  
410 line (iii), it is repeatedly increased by line (xi). The lines (v) - (xix) that follow the **repeat**  
411 in (iv) perform a complete iterative step from  $\mathbf{x}^k$  to  $\mathbf{x}^{k+1}$ , infinite repetitions of such steps  
412 provide the sequence  $R_T = (\mathbf{x}^k)_{k=0}^\infty$ . During one iterative step, there is one application of  
413 the operator  $\mathbf{P}_T$ , in line (xviii), but there are  $N$  steering steps aimed at reducing the value of  
414  $\phi$ ; the latter are done by lines (v) - (xvii). These lines produce a sequence of points  
415  $\mathbf{x}^{k,n}$ , where  $0 \leq n \leq N$  with  $\mathbf{x}^{k,0} = \mathbf{x}^k$ ,  $\mathbf{x}^{k,n} \in \Delta$  and  $\phi(\mathbf{x}^{k,n}) \leq \phi(\mathbf{x}^k)$ .

416     We prove the truth of the last sentence by induction on the nonnegative integers. For  
417  $n = 0$ , we have by lines (v) and (vi) that  $\mathbf{x}^{k,0} = \mathbf{x}^k$ . But  $\mathbf{x}^k \in \Omega$ , since it is either  $\bar{\mathbf{x}}$  that is  
418 assumed to be in  $\Omega$  due to lines (i) and (ii) or it is in the range  $\Omega$  of  $\mathbf{P}_T$  due to lines (xviii)  
419 and (xix). Now we assume, for any  $0 \leq n < N$ , that  $\mathbf{x}^{k,n} \in \Delta$  and  $\phi(\mathbf{x}^{k,n}) \leq \phi(\mathbf{x}^k)$  and  
420 show that lines (viii) - (xvii) perform a computation that leads from  $\mathbf{x}^{k,n}$  to an  $\mathbf{x}^{k,n+1} \in \Delta$   
421 that satisfies  $\phi(\mathbf{x}^{k,n+1}) \leq \phi(\mathbf{x}^k)$ . To see this, observe that line (viii) sets  $\mathbf{v}^{k,n}$  to be a  
422 nonascending vector for  $\phi$  at  $\mathbf{x}^{k,n}$ , which implies that (7) is satisfied with  $\mathbf{x} = \mathbf{x}^{k,n}$  and  
423  $\mathbf{d} = \mathbf{v}^{k,n}$ . Line (ix) sets  $loop$  to *true*, and it remains *true* while searching for the desired  
424  $\mathbf{x}^{k,n+1}$ , by repeatedly executing the loop sequence that follows line (x). In this sequence,  
425 line (xi) increases  $\ell$  by 1 and line (xii) sets  $\beta_{k,n}$  to  $\gamma_\ell$ . Thus for the vector  $\mathbf{z}$  defined by line  
426 (xiii),  $\mathbf{z} \in \Delta$  and  $\phi(\mathbf{z}) \leq \phi(\mathbf{x}^{k,n})$ , provided that  $\beta_{k,n}$  is not greater than the  $\delta$  in (7). Since  
427  $(\gamma_\ell)_{\ell=0}^\infty$  is a summable sequence of positive real numbers, there must be a positive integer  $L$   
428 such that  $\gamma_\ell \leq \delta$ , for all  $\ell \geq L$ . This implies that if we applied lines (xi) - (xiii) often enough,  
429 we would reach a vector  $\mathbf{z}$  that satisfies  $\mathbf{z} \in \Delta$  and  $\phi(\mathbf{z}) \leq \phi(\mathbf{x}^{k,n})$ . If the condition in line  
430 (xiv) is not satisfied when the process gets to it, then lines (xi) - (xiii) are again executed  
431 and eventually we get a vector  $\mathbf{z}$  for which the condition in line (xiv) is satisfied due to the

432 induction hypothesis that  $\phi(\mathbf{x}^{k,n}) \leq \phi(\mathbf{x}^k)$ . By lines (xv) and (xvi) we see that at that  
 433 time  $\mathbf{x}^{k,n+1}$  is set to  $\mathbf{z}$  and so we obtain that  $\mathbf{x}^{k,n+1} \in \Delta$  and  $\phi(\mathbf{x}^{k,n+1}) \leq \phi(\mathbf{x}^k)$ , as desired.  
 434 Line (xvii) sets *loop* to *false* and so control is returned to line (vii). When this happens for  
 435 the  $N$ th time, it will be the case that  $n = N$  and therefore line (xviii) is used to produce  
 436  $\mathbf{x}^{k+1} \in \Omega$  and the increasing of  $k$  by line (xix) allows us then to move on to the next iterative  
 437 step. Infinite repetition of such steps produces the sequence  $R_T = (\mathbf{x}^k)_{k=0}^\infty$  of points in  $\Omega$ .

438 We now show that if  $O\left(T, \varepsilon, \left((\mathbf{P}_T)^k \mathbf{x}\right)_{k=0}^\infty\right)$  is defined for every  $\mathbf{x} \in \Omega$ , then, for any  
 439  $\varepsilon' > \varepsilon$ , the Superiorized Version of Algorithm **P** produces an  $\varepsilon'$ -compatible output. Since **P**  
 440 is assumed to be strongly perturbation resilient, this desired result follows if we can show  
 441 that there exists a summable sequence  $(\beta_k)_{k=0}^\infty$  of nonnegative real numbers and a bounded  
 442 sequence  $(\mathbf{v}^k)_{k=0}^\infty$  of vectors in  $\mathbb{R}^J$  such that (6) is satisfied for all  $k \geq 0$ . In view of line  
 443 (xviii), this is achieved if we can define the  $\beta_k$  and the  $\mathbf{v}^k$  so that  $\mathbf{x}^{k,N} = \mathbf{x}^k + \beta_k \mathbf{v}^k$ . This  
 444 is done by setting

$$\beta_k = \max \{ \beta_{k,n} \mid 0 \leq n < N \}, \quad (8)$$

$$\mathbf{v}^k = \sum_{n=0}^{N-1} \frac{\beta_{k,n}}{\beta_k} \mathbf{v}^{k,n}. \quad (9)$$

445 That these assignments result in  $\mathbf{x}^{k,N} = \mathbf{x}^k + \beta_k \mathbf{v}^k$  follows from lines (v) - (xvii). From line  
 446 (xii) follows that  $(\beta_k)_{k=0}^\infty$  is a subsequence of  $(\gamma_\ell)_{\ell=0}^\infty$  and, hence, it is a summable sequence  
 447 of nonnegative real numbers. Since each  $\|\mathbf{v}^{k,n}\| \leq 1$  by the definition of a nonascending  
 448 vector, it follows from (8) and (9) that  $\|\mathbf{v}^k\| \leq N$  and so  $(\mathbf{v}^k)_{k=0}^\infty$  is bounded. Part of the  
 449 condition expressed in (6) is that, for all  $k \geq 0$ ,  $\mathbf{x}^k + \beta_k \mathbf{v}^k \in \Delta$ . This follows from the fact  
 450 that  $\mathbf{x}^{k,N} = \mathbf{x}^k + \beta_k \mathbf{v}^k$  is assigned its value by line (xvi), but only if the condition expressed  
 451 in line (xiv) is satisfied.

452 In conclusion, we have shown that the superiorized version of a strongly perturbation  
 453 resilient algorithm produces outputs that are essentially as constraints-compatible as those  
 454 produced by the original version of the algorithm. However, due to the repeated steering of  
 455 the process by lines (vii) - (xvii) toward reducing the value of the optimization criterion  $\phi$ ,  
 456 we can expect that the output of the superiorized version will be superior (from the point  
 457 of view of  $\phi$ ) to the output of the original algorithm.



458 **F. Information on performance comparison with MAP methods**

459 Using our notation, the constrained minimization formulation that we are considering is:

460 Given an  $\varepsilon \in \mathbb{R}_+$ ,

$$\text{minimize } \phi(\mathbf{x}), \text{ subject to } \mathcal{P}r_T(\mathbf{x}) \leq \varepsilon. \quad (10)$$

461 The aim of superiorization is not identical with the aim of constrained minimization in (10).

462 One difference is that  $\varepsilon$  is not “given” in the superiorization context. The superiorization

463 of an algorithm produces a sequence and, for any  $\varepsilon$ , the associated output of the algorithm

464 is considered to be the first  $\mathbf{x}$  in the sequence for which  $\mathcal{P}r_T(\mathbf{x}) \leq \varepsilon$ . The other difference

465 is that we do not claim that this output is a minimizer of  $\phi$  among all points that satisfy

466 the constraint, but hope only that it is usually an  $\mathbf{x}$  for which  $\phi(\mathbf{x})$  is at the small end

467 of its range of values over the set of constraint-satisfying points. This latter difference is

468 generally shared by comparisons of a heuristic approach with an exact approach to solving

469 a constrained minimization problem.

470 The MAP (or regularized) formulation of a physical problem that leads to the constrained

471 minimization problem (10) is the unconstrained minimization problem of the form: Given

472 a  $\beta \in \mathbb{R}_+$ ,

$$\text{minimize } [\phi(\mathbf{x}) + \beta \mathcal{P}r_T(\mathbf{x})]. \quad (11)$$

473 Formulations of both kinds (i.e, the ones of (10) and of (11)) are widely used for solving

474 medical physics problems and the question “Which of these two formulations leads to faster or

475 better solutions of the underlying physical problem?” is open. Examples of both formulations

476 with various choices for  $\mathcal{P}r_T$  and  $\phi$  are listed in the beginning parts of the paper of Goldstein

477 and Osher<sup>47</sup>.

478 We now return to the question raised near the end of Section I: Will superiorization pro-

479 duce superior results to those produced by contemporary MAP methods or is it faster than

480 the better of such methods? As yet, there is very little information available regarding this

481 general question; in fact, we are aware of only one published study<sup>45</sup>. That study compared

482 a superiorization algorithm with the algorithm of Goldstein and Osher that they refer to

483 as TwIST<sup>46</sup> with split Bregman<sup>47</sup> as the substep, which is indeed a contemporary method

484 that uses the MAP formulation. (For example, see the discussion of the split Bregman

485 method in<sup>56</sup>.) The problem  $S$  to which the two algorithms were applied was one from the

486 tomographic problem set  $\mathbb{S}$  defined in (1).  $Res_S$  as defined in (2) was used as the proximity

487 function and total variation,  $TV$  as defined below in (12), was the choice for  $\phi$ . It is reported  
 488 in<sup>45</sup> that for the outputs of the two algorithms that were being compared, the values of  $Res_S$   
 489 and  $TV$  were very similar, but the superiorization algorithm produced its output four times  
 490 faster than the MAP method.

### 491 III. AN ILLUSTRATIVE EXAMPLE

#### 492 A. Application to tomography

493 We use *tomography* to refer to the process of reconstructing a function over a Euclidean  
 494 space from estimated values of its integrals along lines (that are usually, but not necessarily,  
 495 straight). The particular reconstruction processes to which our discussion applies are the  
 496 *series expansion methods*, see Section 6.3 of<sup>55</sup>, in which it is assumed that the function to  
 497 be reconstructed can be approximated by a linear combination of a finite number (say  $J$ )  
 498 of basis functions and the reconstruction task becomes one of estimating the coefficients of  
 499 the basis functions in the expansion. Sometimes, prior knowledge about the nature of the  
 500 function to be reconstructed allows us to confine the sought-after vector  $\mathbf{x}$  of coefficients to  
 501 a subset  $\Omega$  of  $\mathbb{R}^J$  (such as the nonnegative orthant  $\mathbb{R}_+^J$ ). We use  $i$  to index the lines along  
 502 which we integrate,  $\mathbf{a}^i \in \mathbb{R}^J$  to denote the vector whose  $j$ th component is the integral of the  
 503  $j$ th basis function along the  $i$ th line, and  $b_i$  to denote the measured integral of the function  
 504 to be reconstructed along the  $i$ th line. Under these circumstances the constraints come from  
 505 the desire that, for each of the lines,  $\langle \mathbf{a}^i, \mathbf{x} \rangle$  should be close (in some sense) to  $b_i$ .

506 To make this concrete, consider (1). Such a description of the constraints arises in  
 507 tomography by grouping the lines of integration into  $W$  blocks, with  $\ell_w$  lines in the  $w$ th block.  
 508 Such groupings often (but not always) are done according to some geometrical condition on  
 509 the lines (for example, in case of straight lines, we may decide that all the lines that are  
 510 parallel to each other form one block). In this framework the proximity function  $Res$  defined  
 511 by (2) provides a reasonable measure of the incompatibility of a vector  $\mathbf{x}$  with the constraints.  
 512 The algorithm  $\mathbf{R}$  described by (3) - (5) is applicable to this concrete formulation.

513 There are many optimization criteria that have been used in tomography, see Section  
 514 6.4 of<sup>55</sup>, here we discuss the one called *total variation* ( $TV$ ), whose use has been popular  
 515 in medical physics recently, see as examples<sup>20,22,23,41-44</sup>. The definition of  $TV$  that we use

516 here requires a certain way of selecting the basis functions. It is assumed that the function  
 517 to be reconstructed is defined in the plane  $\mathbb{R}^2$  and is zero-valued outside a square-shaped  
 518 region in the plane. This region is subdivided into  $J$  smaller equal-sized squares (*pixels*)  
 519 and the  $J$  basis functions are defined by having value one in exactly one pixel and value  
 520 zero everywhere else. We index the pixels by  $j$  and we let  $C$  denote the set of all indices of  
 521 pixels that are not in the rightmost column or the bottom row of the pixel array. For any  
 522 pixel with index  $j$  in  $C$ , let  $r(j)$  and  $b(j)$  be the index of the pixel to its right and below it,  
 523 respectively. We define  $TV : \mathbb{R}^J \rightarrow \mathbb{R}$  by

$$TV(\mathbf{x}) = \sum_{j \in C} \sqrt{(x_j - x_{r(j)})^2 + (x_j - x_{b(j)})^2}. \quad (12)$$

524 The method we adopted to generate a nonascending vector for the  $TV$  function at an  
 525  $\mathbf{x} \in \mathbb{R}^J$  is based on Theorem 2 of the Appendix. It is applicable since  $TV : \mathbb{R}^J \rightarrow \mathbb{R}$  is a  
 526 convex function; see, for example, the end of the Proof of Proposition 1 of<sup>f41</sup>. Now consider  
 527 an integer  $j'$  such that  $1 \leq j' \leq J$ . Looking at the sum in (12), we see that  $x_{j'}$  appears in  
 528 at most three terms, in which  $j'$  must be either  $j$ , or  $r(j)$ , or  $b(j)$  for some  $j \in C$ . By taking  
 529 the formal partial derivatives of these three terms, we see that  $\frac{\partial TV}{\partial x_{j'}}(\mathbf{x})$  is well-defined if the  
 530 denominator in the formal derivative of any of the three terms is not zero for  $\mathbf{x}$ . In view of  
 531 this, we define the  $\mathbf{g}$  in Theorem 2 as follows. If the denominator in any of the three formal  
 532 partial derivatives with respect to  $x_{j'}$  has an absolute value less than a very small positive  
 533 number (we used  $10^{-20}$ ), then we set  $g_{j'}$  to zero, otherwise we set it to  $\frac{\partial TV}{\partial x_{j'}}(\mathbf{x})$ . Clearly  
 534 the resulting  $\mathbf{g} \in \mathbb{R}^J$  satisfies the condition in Theorem 2 and hence provides a  $\mathbf{d}$  that is a  
 535 nonascending vector for  $TV$  at  $\mathbf{x}$ .

536 Previously reported reconstructions using  $TV$ -superiorization selected the  $\mathbf{d}$  using sub-  
 537 gradients as discussed in the paragraph following (7); such a  $\mathbf{d}$  is not guaranteed to be a  
 538 nonascending vector for the  $TV$  function. What we are proposing here is not only mathe-  
 539 matically rigorous (in the sense that it is guaranteed to produce a nonascending vector for  
 540 the  $TV$  function), but it can also lead to a better reconstructions, as illustrated in Subsection  
 541 **IIID**.

542

**B. The data generation for the experiments**

543 The data sets used in the experiments reported in this paper were generated in such a  
544 way that they share the noise-characteristics of CT scanners when used for scanning the  
545 human head and brain; as discussed, for example, in Chapter 5 of<sup>55</sup>. They were generated  
546 using the software SNARK09<sup>57</sup>.

547 The head phantom that was used for data generation is based on an actual cross-section  
548 of the human head. It is described as a collection of geometrical objects (such as ellipses,  
549 triangles and segments of circles) whose combination accurately resembles the anatomical  
550 features of the actual head cross-section. In addition, the basic phantom contains a large  
551 tumor. The actual phantom used was obtained by a random variation of the basic phantom,  
552 by incorporating into it local inhomogeneities and small low-contrast tumors at random  
553 locations. This phantom is represented by the image in figure 1. That image comprises  
554  $485 \times 485$  pixels each of size 0.376 mm by 0.376 mm. The values assigned to the pixels are  
555 obtained by an  $11 \times 11$  sub-sampling of the pixels and averaging the values assigned to the  
556 sub-samples by the geometrical objects that are used to describe the anatomical features  
557 and the tumors. Those values are approximate linear attenuation coefficients per cm at 60  
558 keV (0.416 for bone, 0.210 for brain, 0.207 for cerebrospinal fluid). The contrast of the small  
559 tumors with their background is  $0.003 \text{ cm}^{-1}$ . In order to clearly see the low-contrast details  
560 in the interior of the skull, we use zero (black) to represent the value 0.204 (or anything less)  
561 and 255 (white) to represent 0.21675 or anything more).

562 For the selected head phantom we generated *parallel projection data*, in which one *view*  
563 comprises estimates of integrals through the phantom for a set of 693 equally-spaced parallel  
564 lines with a spacing of 0.0376 cm between them. (We chose to simulate parallel rather  
565 than divergent projection data, since the reconstruction by the method of<sup>42</sup> with which  
566 we wish to compare the superiorization approach were performed for us by the authors  
567 of<sup>42</sup> on parallel data. Even though contemporary CT scanners use divergent projection  
568 data, results obtained by the use of parallel projection data are relevant to them, since it  
569 is known that the quality of reconstructions from these two modes of data collection are  
570 very similar as long as the data generations use similar frequencies of sampling of lines and  
571 similar noise characteristics in the estimated integrals for those lines; see, for example, the  
572 reconstructions from divergent and parallel projection data in figure 5.15 of<sup>55</sup>.) In calculating

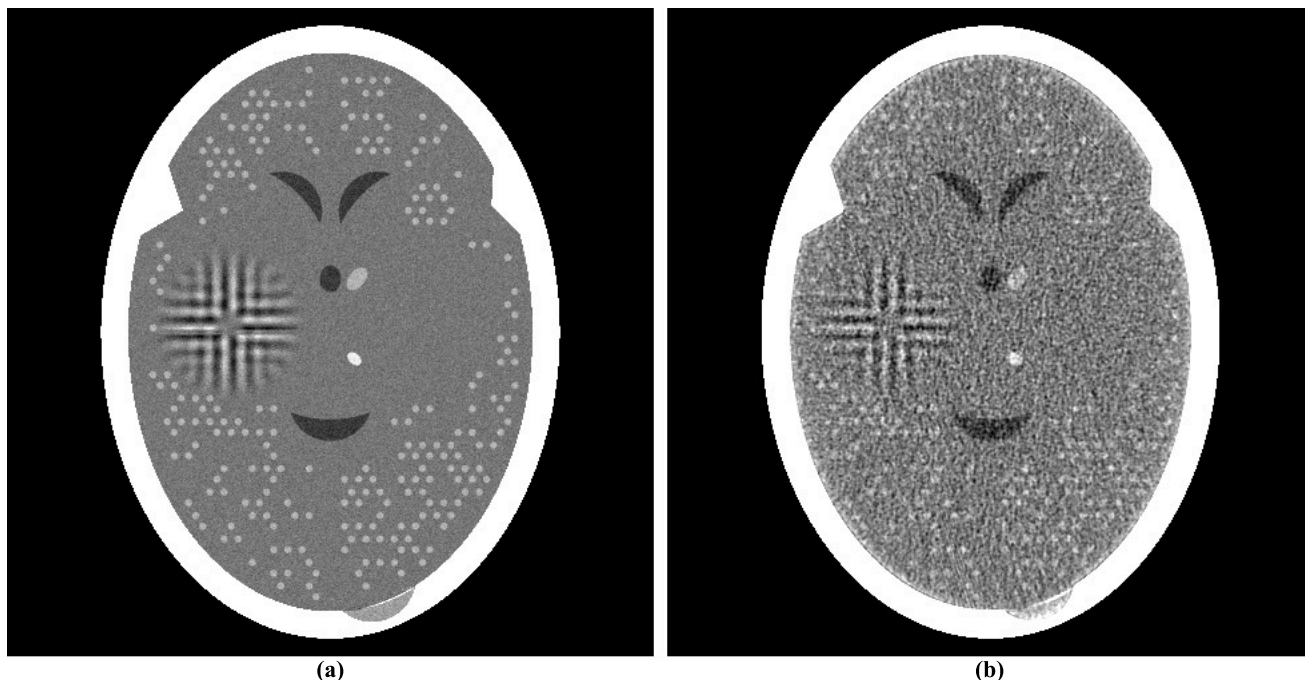


Figure 1: (a) A head phantom. (b) Reconstruction of the head phantom from realistically simulated projection data for 360 views using ART with blob basis functions.

573 these estimates we take into consideration the effects of photon statistics, detector width  
 574 and scatter. Details of how we do this exactly can be found in Sections 5.5 and 5.9 of<sup>55</sup>.  
 575 Briefly, quantum noise is calculated based on the assumption that approximately 2,000,000  
 576 photons enter the head along each ray, detector width is simulated by using 11 sub-rays  
 577 along each of which the attenuation is calculated independently and then combined at the  
 578 detector, and 5% of the photons get counted not by the detector for the ray in question but  
 579 detectors for the neighboring rays. For the experiments in this paper, we did not simulate  
 580 the poly-energetic nature of the x-ray source. To indicate what can be achieved in clinical  
 581 CT, we show in figure 1(b) a reconstruction that was made from data comprising of 360  
 582 such views with the reconstruction algorithm known as ART with blob basis functions; see<sup>55</sup>  
 583 (Chapter 11).

### 584 C. Superiorization reconstruction from a few views

585 The main reason in the literature for advocating the use of  $TV$  as the optimization  
 586 criterion is that by doing so one can achieve efficacious reconstructions even from sparsely

587 sampled data. In our own work<sup>31</sup> with realistically simulated CT data we found that this is  
 588 not always the case and this will be demonstrated again by the experiments reported in the  
 589 current paper.

590 There have appeared in the literature some approaches to  $TV$  minimization that seem  
 591 to indicate a more efficacious performance for CT than the one reported in<sup>31</sup>. One of these  
 592 is the Adaptive Steepest Descent Projections Onto Convex Sets (ASD-POCS) algorithm,  
 593 which is described in detail in the much-cited paper of Sidky and Pan<sup>42</sup> and whose use has  
 594 been since reported in a number of subsequent publications, for example, in<sup>23,43</sup>. We note  
 595 that ASD-POCS was designed with the aim of producing an exact minimization algorithm,  
 596 in contrast to our heuristic superiorization approach. Translating equations (6)-(8) of<sup>42</sup>  
 597 into our terminology, the aim of ASD-POCS is the following: Given an  $\varepsilon \in \mathbb{R}_+$ , find an  
 598  $\varepsilon$ -compatible  $\mathbf{x} \in \Omega = \mathbb{R}_+^J$  for which  $TV(\mathbf{x})$  is minimal. (Note that this aim is a special  
 599 case of the constrained optimization formulation presented in (10).) In order to test ASD-  
 600 POCS, we generated realistic projection data as described in the previous subsection but  
 601 for only 60 views at 3 degree increments with the spacing between the lines for which  
 602 integrals are estimated set at 0.752 mm. Thus the number of rays (and hence the number  
 603 photons put into the head) in this data set is a twelfth of what it is in the data set used to  
 604 produce the reconstruction in figure 1(b). A reconstruction from these data was produced  
 605 for us using ASD-POCS by the authors of<sup>42</sup> (this ensured that it does not suffer due to our  
 606 misinterpretation of the algorithm or from our inappropriate choices of the free parameters),  
 607 it is shown in figure 2(a).

608 Since the image quality of figure 2(a) is not anywhere near to that of figure 1(b), we present  
 609 here a brief discussion as to why we are showing such images. Many publications in the recent  
 610 medical imaging literature have claimed that medically-efficacious reconstructions can be  
 611 obtained by the use of  $TV$ -minimization from data as sparse as what was used to produce  
 612 figure 2(a). (In fact, ASD-POCS was motivated and used with such an aim in mind<sup>23,42,43</sup>.)  
 613 Such publications usually show reconstructions from sparse data as evidence for the validity  
 614 of their claims. They can do this because in their presented illustrations the features that  
 615 are observable in the reconstructions are usually much larger and/or of much higher contrast  
 616 against their backgrounds than the small “tumors” in figure 1(a), which are perfectly visible  
 617 in the reconstruction in figure 1(b), but are not detectable in the reconstruction from sparse  
 618 data in figure 2(a). The reason why that reconstruction appears to be unacceptably bad is

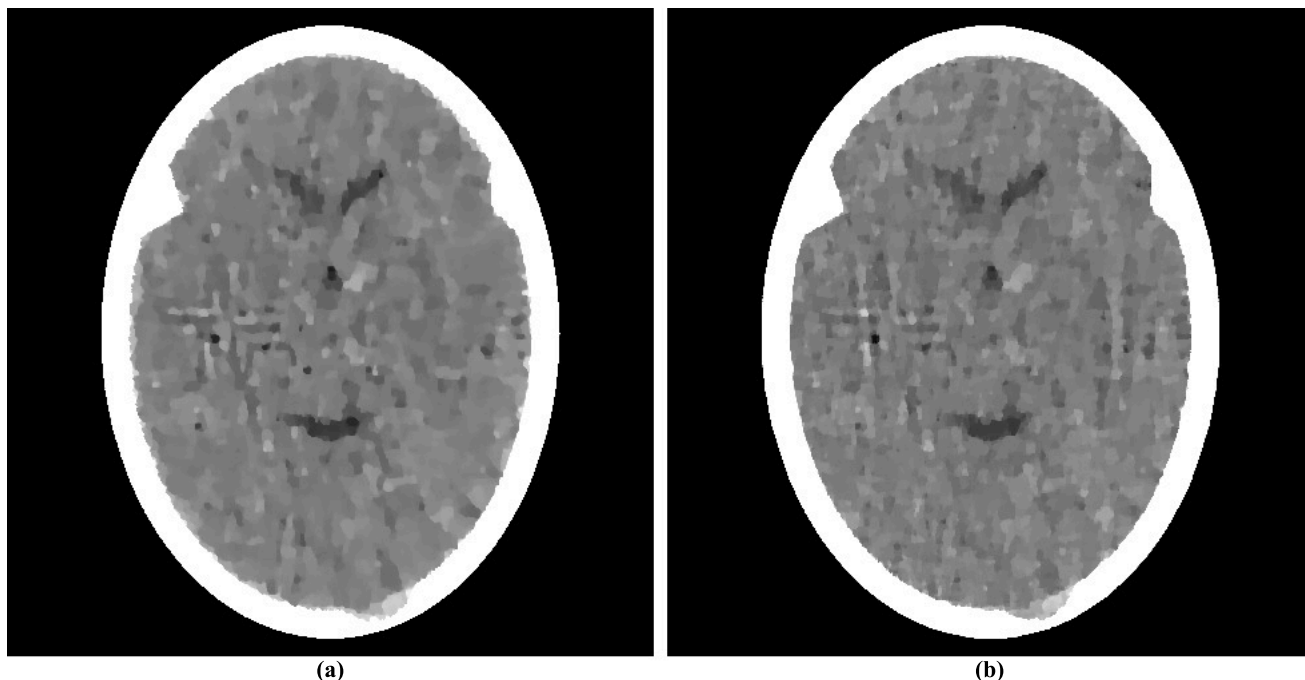


Figure 2: Reconstructions using  $TV$  as the optimization criterion from realistically simulated projection data for 60 views using (a) ASD-POCS and (b) superiorization. As compared to figure 1(b), these reconstructions fail in two ways: they do not show some of the fine details in the phantom and they present some artifactual variations. The former of these is a consequence of reconstructing from a much smaller data set than used for figure 1(b). The latter is due to using a very narrow window (13.5 HU) in these displays. Were we to use a wider display window (e.g., from -429 HU to 429 HU) for the reconstructions in this figure and in figure 1(b), the visual appearance of the resulting images would be nearly indistinguishable.

619 that the display window (from  $0.204 \text{ cm}^{-1}$  linear attenuation coefficient to  $0.21675 \text{ cm}^{-1}$  linear  
 620 attenuation coefficient) is very narrow; it was selected to enhance the visibility of the small  
 621 low-contrast tumors. The width of this window corresponds to about 13.5 Hounsfield Units  
 622 (HU). As compared to this, in their evaluation of sparse-view reconstruction from flat-panel-  
 623 detector cone-beam CT, Bian *et al.*<sup>43</sup> use what they call a “soft-tissue grayscale window”  
 624 (also a “narrow window”) from -429 HU to 429 HU to display head phantom reconstructions.  
 625 Using such a window for our reconstructions shown figures 2(a) and 1(b) would result in  
 626 images that are nearly indistinguishable from each other. Thus reporting the images using  
 627 such a display window is consistent with the claim that a TV-minimizing reconstruction

628 from a few views is similar in quality to a more traditional reconstruction from many views.  
 629 However, our much narrower display window reveals that this is not really so. We therefore  
 630 continue using our much narrower window in what follows, since it clearly reveals the nature  
 631 of the reconstructions being compared, warts and all.

632 While this ASD-POCS reconstruction is not as good as it should be for diagnostic CT of  
 633 the brain (due to the sparsity of the data), it is visually better than the reconstruction using  
 634 superiorization from similar data as reported in<sup>31</sup>. We discuss the reasons for this in the  
 635 next subsection. Here we concentrate on examining whether one can achieve a reconstruction  
 636 using superiorization that is as good as that produced by ASD-POCS from the same data.

637 For this we first need to examine the numerical properties of the ASD-POCS construc-  
 638 tion. This reconstruction uses  $485 \times 485$  pixels each of size 0.376 mm by 0.376 mm. This  
 639 implies that  $J = 235,225$  and it also determines the components of the vectors  $\mathbf{a}^i \in \mathbb{R}^J$  in  
 640 the precise specification of the problem  $S$ . The  $Res_S$ , as defined by (2), of the ASD-POCS  
 641 reconstruction is 0.33 and the  $TV$ , as defined by (12), is 835.

642 We applied to the same problem  $S$  a superiorized version of the algorithm  $\mathbf{R}$  defined  
 643 by (3). To complete the specification of  $\mathbf{R}$ , we point out that for the ordering of views we  
 644 chose the “efficient” one that was introduced in<sup>58</sup> and is also discussed on page 209 of<sup>55</sup>.  
 645 The choices we made for the superiorization are the following:  $\gamma_\ell = 0.99995^\ell$ ,  $\bar{\mathbf{x}}$  is the zero  
 646 vector and  $N = 20$ . The nonascending vector was computed by the method described in the  
 647 paragraph below (12). Denoting by  $R_S$  the infinite sequence of points in  $\Omega$  that is produced  
 648 by the superiorized version of the algorithm  $\mathbf{R}$  when applied to the problem  $S$ , we chose as  
 649 our reconstruction  $\mathbf{x}^* = O(S, 0.33, R_S)$ . For such a reconstruction we have, by the definition  
 650 of  $O$ , that  $Res_S(\mathbf{x}^*) \leq 0.33$ ; in other words, the output of the superiorization algorithm is  
 651 at least as constraints-compatible with  $S$  as the output of ASD-POCS. From the point of  
 652 view of  $TV$ -minimization, our  $\mathbf{x}^*$  is slightly better:  $TV(\mathbf{x}^*) = 826$ .

653 The superiorization reconstruction is displayed in figure 2(b). Visually it is similar to the  
 654 reconstruction produced by ASD-POCS. From the optimization point of view it achieves the  
 655 desired aim better than ASD-POCS does, since it results in smaller values for both  $Res_S$   
 656 and for  $TV$ , even though only slightly.

657 That the two reconstructions in figure 2 are very similar is not surprising because a  
 658 comparison of the pseudo-codes reveals that the ASD-POCS algorithm in<sup>42</sup> is essentially a  
 659 special case of the Superiorized Version of Algorithm  $\mathbf{P}$ , even though it has been derived



660 from rather different principles. To obtain the ASD-POCS algorithm from our methodology  
 661 described here, we would have to choose an Algebraic Reconstruction Technique (ART;  
 662 see Chapter 11 of<sup>55</sup>) as the algorithm that we are superiorizing. Such a superiorization of  
 663 ART was reported in the earliest paper on superiorization<sup>27</sup>. For the illustration in our  
 664 current paper we decided to superiorize the block-iterative algorithm  $\mathbf{R}$  defined by (3).  
 665 This illustrates the generality of the superiorization approach: it is applicable not only to  
 666 a large class of constrained optimization problems, but also enables the use of any of a  
 667 large class of iterative algorithms designed to produce a constraints-compatible solutions.  
 668 A recent publication aimed at producing an exact  $TV$ -minimizing algorithm based on the  
 669 block-iterative approach is<sup>44</sup>.

#### 670 **D. Effects of variations in the reconstruction approach**

671 The reconstruction in figure 2(a) produced by ASD-POCS definitely “looks better” than  
 672 a reconstruction in<sup>31</sup>, which was obtained using superiorization from similar data. Since, as  
 673 discussed in the last paragraph of the previous subsection, the ASD-POCS algorithm in<sup>42</sup>  
 674 can be obtained as a special case of superiorization, it must be that some of the choices made  
 675 in the details of the implementations are responsible for the visual differences. An analysis  
 676 of the implementational details adopted by the two approaches revealed several differences.  
 677 After removing these differences, the superiorization approach produced the image in figure  
 678 2(b), which is very similar to the reconstruction produced by ASD-POCS. We now list the  
 679 implementational choices that were made for superiorization to make its performance match  
 680 that of the reported implementation of ASD-POCS.

681 One implementational difference is in the stopping-rule of the iterative algorithm; that  
 682 is, the choice of  $\varepsilon$  in determining the output  $O(S, \varepsilon, R_S)$ . Since the data are noisy, the  
 683 phantom itself does not match the data exactly. In previously reported implementations of  
 684 superiorization it was assumed that the iterative process should terminate when an image  
 685 is obtained that is approximately as constraints-compatible as the phantom; in the case of  
 686 the phantom and the projections data on which we report here the value of  $Res_S$  for the  
 687 phantom is approximately 0.91, which is larger than its value (0.33) for the reconstruction  
 688 produced by ASD-POCS. The output  $O(S, 0.91, R_S)$  is shown in figure 3(a). This is a  
 689 wonderfully smooth reconstruction, its  $TV$  value is only 771. However this smoothness

690 comes at a price: we loose not only the ability to detect the large tumor, but we cannot  
 691 even see anatomic features (such as the ventricular cavities) inside the brain. So it appears  
 692 that, in order to see medically-relevant features in the brain, *over-fitting* (in the sense of  
 693 producing a reconstruction from noisy data that is more constraints-compatible than the  
 694 phantom) is desirable.

695 In the implementations that produced previously reported reconstructions by superior-  
 696 ization, the number  $N$  in the Superiorized Version of Algorithm **P** was always chosen to  
 697 be 1. It is possible that this is the wrong choice, making only this change to what lead to  
 698 the reconstruction in figure 2(b) results in the reconstruction shown in figure 3(b). That  
 699 image appears similar to the image in figure 2(b), but it has a higher  $TV$  value, namely 832,  
 700 which is still very slightly lower than that of the ASD-POCS reconstruction. The choice  
 701  $N = 20$  was based on the desire to maintain consistency with what has been practiced using  
 702 ASD-POCS, see page 4790 of<sup>42</sup>. It appears that in the context of our paper the additional  
 703 computing cost due to choosing  $N$  to be 20 rather than 1 is not really justified. (We note  
 704 that if  $\mathbf{d}$  is selected using subgradients as discussed in the paragraph following (7) and thus  
 705  $\mathbf{d}$  is not guaranteed to be a nonascending vector for the  $TV$  function, then the choice of  
 706 20 rather than 1 for  $N$  results in a considerable improvement. However, an even greater  
 707 improvement is achieved even with  $N = 1$  by selecting  $\mathbf{d}$  as recommended in this paper.)

708 Another important difference between the ASD-POCS implementation and the previous  
 709 implementations of the superiorization approach is the size of the pixels in the reconstruc-  
 710 tions. For the ASD-POCS reconstruction this was selected to be 0.376 mm by 0.376 mm.  
 711 In previously reported reconstructions by superiorization it was assumed that the edge of  
 712 a pixel should be the same as the distance between the parallel lines along which the data  
 713 are collected; that is, 0.752 mm for our problem  $S$ . This assumption proved to be false.  
 714  $TV$ -minimization takes care of undesirable artifacts that may otherwise arise due to the  
 715 smaller pixels and this leads to a visual improvement. A superiorizing reconstruction with  
 716 the larger pixels, using  $\varepsilon = 0.33$  and  $N = 20$ , is shown in figure 3(c). (We note that the use  
 717 of smaller pixels during iterative x-ray CT reconstructions was also suggested in<sup>59</sup>. How-  
 718 ever, that approach is quite different from what is presented here: its final result uses larger  
 719 pixels whose values are obtained by averaging assemblies of values provided by the iterative  
 720 process to the smaller pixels. There is no such downsampling in our approach, our final  
 721 result is presented using the smaller pixels. Its smoothness is due to reduction of  $TV$  by the

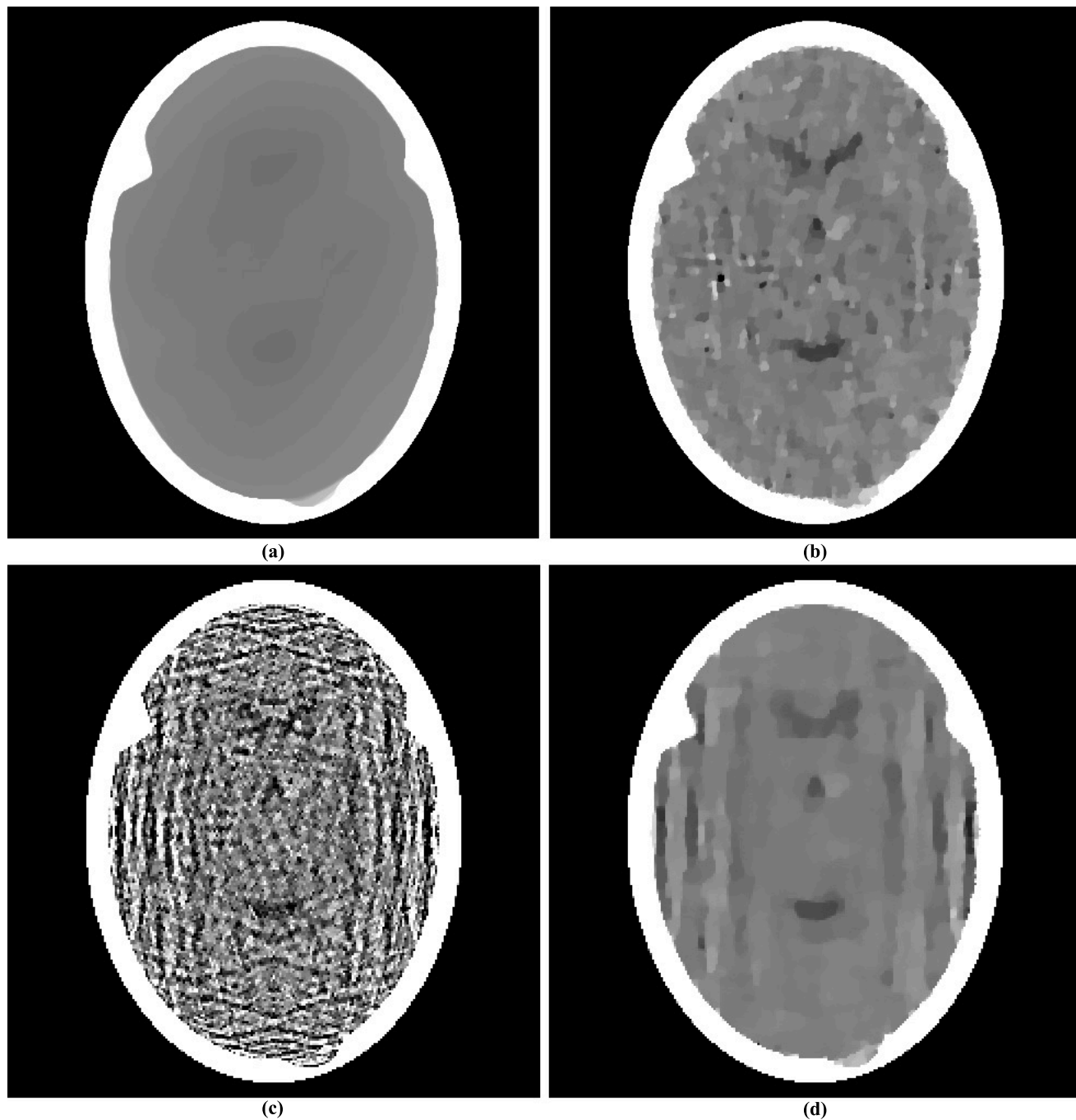


Figure 3: Reconstructions produced by varying some of the parameters in the algorithm that produced figure 2(b). (a) Changing the termination criterion from  $\varepsilon = 0.33$  to  $\varepsilon = 0.91$ . (b) Changing the value of  $N$  from 20 to 1. (c) Reconstructing with pixel size 0.752 mm by 0.752 mm instead of 0.376 mm by 0.376 mm. (d) Reconstructing with all the three changes of (a)-(c).

722 superiorization approach rather than to averaging pixel values in a denser digitization.)

723 Combining the use of the larger pixels with  $\varepsilon = 0.91$  and  $N = 1$  results in the reconstruc-  
 724 tion shown in figure 3(d). This reconstruction, for which the superiorization options were  
 725 selected according to what was done in<sup>31</sup>, is visually inferior to those shown in our figure  
 726 2. The reconstructions displayed in figure 3 also illustrate another important point, namely  
 727 that even though the mathematical results discussed in this paper are valid for a large range  
 728 of choices of the parameters in the superiorization algorithms, for medical efficacy of the  
 729 reconstructions attention has to be paid to these choices since they can have a drastic effect  
 730 on the quality of the reconstruction.

731 It has been mentioned in Subsection II B that except for the presence of  $\mathbf{Q}$  in (3), which  
 732 enforces nonnegativity of the components,  $\mathbf{R}$  is identical to the algorithm used and illustrated  
 733 in<sup>31</sup>. It is known that CT reconstruction of the brain from many views does not suffer  
 734 from ignoring the fact that the components of the  $\mathbf{x}$ , which represent linear attenuation  
 735 coefficients, should be nonnegative; as is illustrated in figure 1(b). This remains so when  
 736 reconstructing from a few views using the method and data that we have been discussing:  
 737 if we do everything in exactly the same way as was done to obtain the reconstruction with  
 738  $TV$  value 826 that is shown in our figure 2(b) but remove  $\mathbf{Q}$  from (3), then we obtain a  
 739 reconstruction in figure 4(a) whose  $TV$  value is 829.

740 Another variation that deserves discussion, because it has been suggested in the  
 741 literature<sup>22</sup>, is one that does not come about by making choices for the general approach of  
 742 the Superiorized Version of Algorithm  $\mathbf{P}$  but rather by changing the nature of the approach.  
 743 The variation in question is not applicable in general, but can be applied to the special  
 744 case when the algorithm to be superiorized is the  $\mathbf{R}$  defined by (3). It was suggested as  
 745 an improvement to the approach presented above with the choice  $N = 1$ . The idea was  
 746 based on recognizing the block-iterative nature of the algorithmic operator  $\mathbf{R}_S$  in (3) and  
 747 intermingling the perturbation steps of lines (vii)-(xvii) of the Superiorized Version of Al-  
 748 gorithm  $\mathbf{R}$  with the projection steps  $\mathbf{B}_{S_1}, \dots, \mathbf{B}_{S_W}$  of (3). It was reported in<sup>22</sup> that doing  
 749 this is advantageous to using the Superiorized Version of Algorithm  $\mathbf{R}$ . However, when we  
 750 applied the variation of the Superiorized Version of Algorithm  $\mathbf{R}$  that is proposed in<sup>22</sup> to  
 751 the problem  $S$  that we have been using in this section, we ended up with the reconstruction  
 752 in figure 4(b) whose  $TV$  value is 920. This is not as good as what was obtained using the  
 753 version of the algorithm that produced the reconstruction in figure 2(b). We conclude that

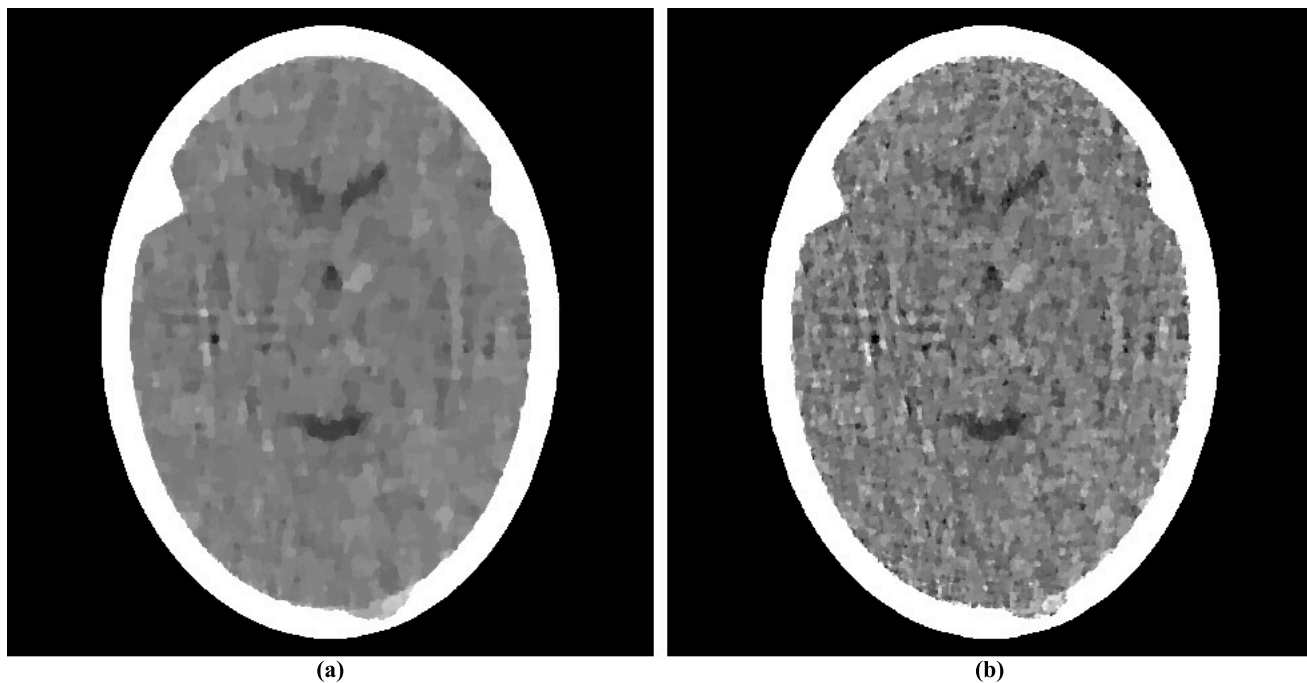


Figure 4: Reconstructions by variations that do not fit into the framework within which the previously shown reconstructions were produced. (a) Not using nonnegativity in the algorithm. (b) Interleaving perturbations with blocks.

754 the variation suggested by<sup>22</sup>, which does not fit into the theory of our paper, does not have  
 755 an advantage over what we are proposing here, at least for the problem  $S$  that we have  
 756 been discussing in this section. We conjecture that the improvement reported in<sup>22</sup> is due to  
 757 selecting  $\mathbf{d}$  using subgradients as discussed in the paragraph following (7) and, as discussed  
 758 earlier, such an improvement is not obtained if  $\mathbf{d}$  is selected by the more appropriate method  
 759 recommended in this paper.

760

#### IV. DISCUSSION AND CONCLUSIONS

761 Constrained optimization is an often-used tool in medical physics. The methodology of  
 762 superiorization is a heuristic (as opposed to exact) approach to constrained optimization.

763 Although the idea of superiorization was introduced in 2007 and its practical use has been  
 764 demonstrated in several publications since, this paper is the first to provide a solid math-  
 765 ematical foundation to superiorization as applied to the noisy problems of the real world.  
 766 These foundations include a precise definition of constraints-compatibility, the concept of a

767 strongly perturbation resilient algorithm, simple conditions that ensure that an algorithm  
 768 is strongly perturbation resilient, the superiorized version of an algorithm and the showing  
 769 that the superiorized version of a strongly perturbation resilient algorithm produces outputs  
 770 that are essentially as constraints-compatible as those produced by the original version but  
 771 are likely to have a smaller value of the chosen optimization criterion.

772 The approach is very general. For any iterative algorithm  $\mathbf{P}$  and for any optimization  
 773 criterion  $\phi$  for which we know how to produce nonascending vectors, the pseudocode given  
 774 in Subsection IIE automatically provides the version of  $\mathbf{P}$  that is superiorized for  $\phi$ .

775 We demonstrated superiorization for tomography when total variation is used as the  
 776 optimization criterion. In particular, we illustrated on a particular tomography problem  
 777 that, in spite of its generality, superiorization produced a reconstruction that is as good  
 778 as (from the points of view of constraints-compatibility and  $TV$ -minimization) what was  
 779 obtained by the ASD-POCS algorithm that was specially designed for  $TV$ -minimization in  
 780 tomography.

## 781 Acknowledgments

782 The detailed and penetrating comments of three reviewers and the editors helped us to  
 783 improve this paper in a significant way. We thank Prof. Xiaochuan Pan and his coworkers  
 784 from the University of Chicago for providing us with the reconstruction from our data using  
 785 their implementation of their ASD-POCS algorithm. Our work is supported by the Na-  
 786 tional Science Foundation award number DMS-1114901, the United States-Israel Binational  
 787 Science Foundation (BSF) grant number 200912, and the US Department of Army award  
 788 number W81XWH-10-1-0170.

## 789 Appendix

### 790 Conditions for strong perturbation resilience

791 *Theorem 1.* Let  $\mathbf{P}$  be an algorithm for a problem structure  $\langle \mathbb{T}, \mathcal{P}r \rangle$  such that, for all  
 792  $T \in \mathbb{T}$ ,  $\mathbf{P}$  is boundedly convergent for  $T$ ,  $\mathcal{P}r_T : \Omega \rightarrow \mathbb{R}$  is uniformly continuous and  
 793  $\mathbf{P}_T : \Delta \rightarrow \Omega$  is nonexpansive. Then  $\mathbf{P}$  is strongly perturbation resilient.

794 *Proof.* We first show that there exists an  $\varepsilon \in \mathbb{R}_+$  such that  $O\left(T, \varepsilon, \left((\mathbf{P}_T)^k \mathbf{x}\right)_{k=0}^{\infty}\right)$   
 795 is defined for every  $\mathbf{x} \in \Omega$ . Under the assumptions of the theorem, let  $\gamma \in \mathbb{R}_+$  be such  
 796 that  $\mathcal{P}r_T(\mathbf{y}(\mathbf{x})) \leq \gamma$ , for every  $\mathbf{x} \in \Omega$ . We prove that  $O\left(T, 2\gamma, \left((\mathbf{P}_T)^k \mathbf{x}\right)_{k=0}^{\infty}\right)$  is defined  
 797 for every  $\mathbf{x} \in \Omega$  as follows. Select a particular  $\mathbf{x} \in \Omega$ . By uniform continuity of  $\mathcal{P}r_T$ ,  
 798 there exists a  $\delta > 0$ , such that  $|\mathcal{P}r_T(\mathbf{z}) - \mathcal{P}r_T(\mathbf{y}(\mathbf{x}))| \leq \gamma$ , for any  $\mathbf{z} \in \Omega$  for which  
 799  $\|\mathbf{z} - \mathbf{y}(\mathbf{x})\| \leq \delta$ . Since  $\mathbf{P}$  is convergent for  $T$ , there exists a nonnegative integer  $K$ , such  
 800 that  $\left\|(\mathbf{P}_T)^K \mathbf{x} - \mathbf{y}(\mathbf{x})\right\| \leq \delta$ . It follows that

$$\begin{aligned} \left| \mathcal{P}r_T\left((\mathbf{P}_T)^K \mathbf{x}\right) \right| &\leq \left| \mathcal{P}r_T\left((\mathbf{P}_T)^K \mathbf{x}\right) - \mathcal{P}r_T(\mathbf{y}(\mathbf{x})) \right| + |\mathcal{P}r_T(\mathbf{y}(\mathbf{x}))| \\ &\leq 2\gamma. \end{aligned} \quad (13)$$

801 Now let  $T \in \mathbb{T}$  and  $\varepsilon \in \mathbb{R}_+$  be such that  $O\left(T, \varepsilon, \left((\mathbf{P}_T)^k \mathbf{x}\right)_{k=0}^{\infty}\right)$  is defined for every  
 802  $\mathbf{x} \in \Omega$ . To prove the theorem, we need to show that  $O\left(T, \varepsilon', R\right)$  is defined for every  $\varepsilon' > \varepsilon$   
 803 and for every sequence  $R = \left(\mathbf{x}^k\right)_{k=0}^{\infty}$  of points in  $\Omega$  for which, for all  $k \geq 0$ , (6) is satisfied for  
 804 bounded perturbations  $\beta_k \mathbf{v}^k$ . Let  $\varepsilon'$  and  $R$  satisfy the conditions of the previous sentence.

For  $k \geq 0$ , we have, due to the nonexpansiveness of  $\mathbf{P}_T$ , that

$$\left\| \mathbf{x}^{k+1} - \mathbf{P}_T \mathbf{x}^k \right\| = \left\| \mathbf{P}_T \left( \mathbf{x}^k + \beta_k \mathbf{v}^k \right) - \mathbf{P}_T \mathbf{x}^k \right\| \leq \left\| \beta_k \mathbf{v}^k \right\|. \quad (14)$$

805 Denote  $\left\| \beta_k \mathbf{v}^k \right\|$  by  $r_k$ . Clearly,  $r_k \in \mathbb{R}_+$  and it follows from the definition of bounded  
 806 perturbations that  $\sum_{k=0}^{\infty} r_k < \infty$ .

807 We next prove by induction that, for every pair of nonnegative integers  $k$  and  $i$ ,

$$\left\| \mathbf{x}^{k+i} - (\mathbf{P}_T)^i \mathbf{x}^k \right\| \leq \sum_{j=k}^{k+i-1} r_j. \quad (15)$$

808 Let  $k$  be an arbitrary nonnegative integer. If  $i = 0$ , then the value is zero on both sides of  
 809 the inequality and hence (15) holds. Now assume that (15) holds for an integer  $i \geq 0$ . Then,  
 810 by (14) and the nonexpansiveness of  $\mathbf{P}_T$ ,

$$\begin{aligned} \left\| \mathbf{x}^{k+i+1} - (\mathbf{P}_T)^{i+1} \mathbf{x}^k \right\| &\leq \left\| \mathbf{x}^{k+i+1} - \mathbf{P}_T \mathbf{x}^{k+i} \right\| \\ &\quad + \left\| \mathbf{P}_T \mathbf{x}^{k+i} - (\mathbf{P}_T)^{i+1} \mathbf{x}^k \right\| \\ &\leq r_{k+i} + \left\| \mathbf{x}^{k+i} - (\mathbf{P}_T)^i \mathbf{x}^k \right\| \\ &\leq r_{k+i} + \sum_{j=k}^{k+i-1} r_j \\ &= \sum_{j=k}^{k+i} r_j, \end{aligned} \quad (16)$$

811 which completes our inductive proof. A consequence of (15) is that, for every pair of non-  
812 negative integers  $k$  and  $i$ ,

$$\left\| \mathbf{x}^{k+i} - (\mathbf{P}_T)^i \mathbf{x}^k \right\| \leq \sum_{j=k}^{\infty} r_j. \quad (17)$$

813 Due to the summability of the nonnegative sequence  $(r_k)_{k=0}^{\infty}$ , the right-hand side (and hence  
814 the left-hand side) of this inequality gets arbitrarily close to zero as  $k$  increases.

815 Since  $\mathcal{P}r_T$  is uniformly continuous, there exists a  $\delta$  such that, for all  $\mathbf{x}, \mathbf{y} \in \Omega$ ,  
816  $|\mathcal{P}r_T(\mathbf{x}) - \mathcal{P}r_T(\mathbf{y})| \leq \varepsilon' - \varepsilon$  provided that  $\|\mathbf{x} - \mathbf{y}\| \leq \delta$ . Select a  $k$  so that  $\sum_{j=k}^{\infty} r_j \leq \delta$ .  
817 By the assumption that  $O\left(T, \varepsilon, \left((\mathbf{P}_T)^k \mathbf{x}\right)_{k=0}^{\infty}\right)$  is defined for every  $\mathbf{x} \in \Omega$ , there exists a  
818 nonnegative integer  $i$  for which  $\mathcal{P}r\left((\mathbf{P}_T)^i \mathbf{x}^k\right) \leq \varepsilon$ . From (17) we have, for this  $k$  and  $i$ ,  
819 that  $\left\| \mathbf{x}^{k+i} - (\mathbf{P}_T)^i \mathbf{x}^k \right\| \leq \delta$  and, hence,

$$\begin{aligned} |\mathcal{P}r_T(\mathbf{x}^{k+i})| &\leq \left| \mathcal{P}r_T(\mathbf{x}^{k+i}) - \mathcal{P}r_T\left((\mathbf{P}_T)^i \mathbf{x}^k\right) \right| \\ &\quad + \left| \mathcal{P}r_T\left((\mathbf{P}_T)^i \mathbf{x}^k\right) \right| \\ &\leq (\varepsilon' - \varepsilon) + \varepsilon = \varepsilon', \end{aligned} \quad (18)$$

820 proving that  $O(T, \varepsilon', R)$  is defined.  $\square$

## 821 Nonascending vectors for convex functions

822 *Theorem 2.* Let  $\phi : \mathbb{R}^J \rightarrow \mathbb{R}$  be a convex function and let  $\mathbf{x} \in \mathbb{R}^J$ . Let  $\mathbf{g} \in \mathbb{R}^J$  satisfy the  
823 property: For  $1 \leq j \leq J$ , if the  $j$ th component  $g_j$  of  $\mathbf{g}$  is not zero, then the partial derivative  
824  $\frac{\partial \phi}{\partial x_j}(\mathbf{x})$  of  $\phi$  at  $\mathbf{x}$  exists and its value is  $g_j$ . Define  $\mathbf{d}$  to be the zero vector if  $\|\mathbf{g}\| = 0$  and to  
825 be  $-\mathbf{g}/\|\mathbf{g}\|$  otherwise. Then  $\mathbf{d}$  is a nonascending vector for  $\phi$  at  $\mathbf{x}$ .

826 *Proof.* The theorem is trivially true if  $\|\mathbf{g}\| = 0$ , so we assume that this is not the case.  
827 We denote by  $I$  the nonempty set of those indices  $j$  for which  $g_j \neq 0$ .

828 For  $1 \leq j \leq J$ , let  $s_j$  be  $g_j/|g_j|$  for  $j \in I$  and be 0 otherwise, and let  $\mathbf{e}^j \in \mathbb{R}^J$  be the vector  
829 all of whose components are zero except for the  $j$ th, which is one. Then, for  $1 \leq j \leq J$ ,  
830 there exists a  $\delta_j > 0$  such that, for  $0 \leq \lambda_j \leq \delta_j$ ,

$$\phi(\mathbf{x} - \lambda_j s_j \mathbf{e}^j) \leq \phi(\mathbf{x}). \quad (19)$$

831 This is obvious if  $s_j = 0$ . Otherwise,  $\frac{\partial \phi}{\partial x_j}(\mathbf{x})$  exists and indicates  $\phi$  increases at  $\mathbf{x}$  if  $s_j = 1$   
832 or that  $\phi$  decreases at  $\mathbf{x}$  if  $s_j = -1$ . The existence of the desired  $\delta_j$  can be derived from the  
833 standard definition of the partial derivative as a limit.



834 We define  $\delta > 0$  by

$$\delta = \frac{\|\mathbf{g}\|}{J} \min_{j \in I} \left\{ \frac{\delta_j}{|g_j|} \right\}. \quad (20)$$

835 Then we have that, for  $0 \leq \lambda \leq \delta$ ,

$$\begin{aligned} \phi(\mathbf{x} + \lambda \mathbf{d}) &= \phi \left( \mathbf{x} - \lambda \sum_{j=1}^J \frac{|g_j|}{\|\mathbf{g}\|} s_j \mathbf{e}^j \right) \\ &= \phi \left( \sum_{j=1}^J \frac{1}{J} \left( \mathbf{x} - \lambda J \frac{|g_j|}{\|\mathbf{g}\|} s_j \mathbf{e}^j \right) \right) \\ &\leq \frac{1}{J} \sum_{j=1}^J \phi \left( \mathbf{x} - \lambda J \frac{|g_j|}{\|\mathbf{g}\|} s_j \mathbf{e}^j \right) \\ &\leq \frac{1}{J} \sum_{j=1}^J \phi(\mathbf{x}) \\ &= \phi(\mathbf{x}). \end{aligned} \quad (21)$$

836 The first inequality above follows from the convexity of  $\phi$  and the second one follows from  
 837 (19), with  $\lambda_j$  defined to be  $\lambda J \frac{|g_j|}{\|\mathbf{g}\|}$ , combined with (20). Thus  $\mathbf{d}$  is a nonascending vector for  
 838  $\phi$  at  $\mathbf{x}$ .  $\square$

839 \* Author to whom correspondence should be addressed; Electronic address: [gaborther-](mailto:gabortherman@yahoo.com)  
 840 [man@yahoo.com](mailto:gabortherman@yahoo.com); URL: <http://www.dig.cs.gc.cuny.edu/~gabor/index.html>

841 <sup>1</sup> J. O. Deasy, “Multiple local minima in radiotherapy optimization problems with dose-volume  
 842 constraints,” *Med. Phys.* **24**, 1157–1161, (1997).

843 <sup>2</sup> G. A. Ezzell, “Genetic and geometric optimization of three-dimensional radiation therapy treat-  
 844 ment planning,” *Med. Phys.* **23**, 293–305, (1996).

845 <sup>3</sup> A. Gustafsson, B. K. Lind, and A. Brahme, “A generalized pencil beam algorithm for optimiza-  
 846 tion of radiation-therapy,” *Med. Phys.* **21**, 343–357, (1994).

847 <sup>4</sup> A. Gustafsson, B. K. Lind, R. Svensson, and A. Brahme, “Simultaneous-optimization of dynamic  
 848 multileaf collimation and scanning patterns or compensation filters using a generalized pencil  
 849 beam algorithm,” *Med. Phys.* **22**, 1141–1156, (1995).

850 <sup>5</sup> E. Lessard and J. Pouliot, “Inverse planning anatomy-based dose optimization for hdr-  
 851 brachytherapy of the prostate using fast simulated annealing algorithm and dedicated objective  
 852 function,” *Med. Phys.* **28**, 773–779, (2001).

- 853 <sup>6</sup> R. Manzke, M. Grass, T. Nielsen, G. Shechter, and D. Hawkes, “Adaptive temporal resolution  
854 optimization in helical cardiac cone beam CT reconstruction,” *Med. Phys.* **30**, 3072–3080, (2003).
- 855 <sup>7</sup> A. B. Pugachev, A. L. Boyer, and L. Xing, “Beam orientation optimization in intensity-  
856 modulated radiation treatment planning,” *Med. Phys.* **27**, 1238–1245, (2000).
- 857 <sup>8</sup> D. M. Shepard, M. A. Earl, X. A. Li, S. Naqvi, and C. Yu, “Direct aperture optimization: A  
858 turnkey solution for step-and-shoot IMRT,” *Med. Phys.* **29**, 1007–1018, (2002).
- 859 <sup>9</sup> C. Studholme, D. L. G. Hill, and D. J. Hawkes, “Automated three-dimensional registration of  
860 magnetic resonance and positron emission tomography brain images by multiresolution opti-  
861 mization of voxel similarity measures,” *Med. Phys.* **24**, 25–35, (1997).
- 862 <sup>10</sup> Q. W. Wu and R. Mohan, “Algorithms and functionality of an intensity modulated radiotherapy  
863 optimization system,” *Med. Phys.* **27**, 701–711, (2000).
- 864 <sup>11</sup> Y. Yu and M. C. Schell, “A genetic algorithm for the optimization of prostate implants,” *Med.*  
865 *Phys.* **23**, 2085–2091, (1996).
- 866 <sup>12</sup> T. Z. Zhang, R. Jeraj, H. Keller, W. G. Lu, G. H. Olivera, T. R. McNutt, T. R. Mackie, and  
867 B. Paliwal, “Treatment plan optimization incorporating respiratory motion,” *Med. Phys.* **31**,  
868 1576–1586, (2004).
- 869 <sup>13</sup> M. Abdoli, M. R. Ay, A. Ahmadian, R. A. Dierckx, and H. Zaidi, “Reduction of dental fill-  
870 ing metallic artifacts in CT-based attenuation correction of PET data using weighted virtual  
871 sinograms optimized by a genetic algorithm,” *Med. Phys.* **37**, 6166–6177, (2010).
- 872 <sup>14</sup> S. Bartolac, S. Graham, J. Siewerdsen, and D. Jaffray, “Fluence field optimization for noise and  
873 dose objectives in CT,” *Med. Phys.* **38**, S2–S17, (2011).
- 874 <sup>15</sup> W. Chen, D. Craft, T. M. Madden, K. Zhang, H. M. Kooy, and G. T. Herman, “A fast opti-  
875 mization algorithm for multicriteria intensity modulated proton therapy planning,” *Med. Phys.*  
876 **37**, 4938–4945, (2010).
- 877 <sup>16</sup> J. Fiege, B. McCurdy, P. Potrebko, H. Champion, and A. Cull, “PARETO: A novel evolutionary  
878 optimization approach to multiobjective IMRT planning,” *Med. Phys.* **38**, 5217–5229, (2011).
- 879 <sup>17</sup> A. Fredriksson, A. Forsgren, and B. Hardemark, “Minimax optimization for handling range and  
880 setup uncertainties in proton therapy,” *Med. Phys.* **38**, 1672–1684, (2011).
- 881 <sup>18</sup> C. Holdsworth, M. Kim, J. Liao, and M. H. Phillips, “A hierarchical evolutionary algorithm for  
882 multiobjective optimization in IMRT,” *Med. Phys.* **37**, 4986–4997, (2010).
- 883 <sup>19</sup> C. Holdsworth, R. D. Stewart, M. Kim, J. Liao, and M. H. Phillips, “Investigation of effective

- 884 decision criteria for multiobjective optimization in IMRT,” *Med. Phys.* **38**, 2964–2974, (2011).
- 885 <sup>20</sup> T. Kim, L. Zhu, T.-S. Suh, S. Geneser, B. Meng, and L. Xing, “Inverse planning for IMRT with  
886 nonuniform beam profiles using total-variation regularization (TVR),” *Med. Phys.* **38**, 57–66,  
887 (2011).
- 888 <sup>21</sup> C. Men, H. E. Romeijn, X. Jia, and S. B. Jiang, “Ultrafast treatment plan optimization for  
889 volumetric modulated arc therapy (VMAT),” *Med. Phys.* **37**, 5787–5791, (2010).
- 890 <sup>22</sup> S. N. Penfold, R. W. Schulte, Y. Censor, and A. B. Rosenfeld, “Total variation superiorization  
891 schemes in proton computed tomography image reconstruction,” *Med. Phys.* **37**, 5887–5895,  
892 (2010).
- 893 <sup>23</sup> E. Y. Sidky, Y. Duchin, X. Pan, and C. Ullberg, “A constrained, total-variation minimization  
894 algorithm for low-intensity x-ray CT,” *Med. Phys.* **38**, S117–S125, (2011).
- 895 <sup>24</sup> H. Stabenau, L. Rivera, E. Yorke, J. Yang, R. Lu, R. J. Radke, and A. Jackson, “Reduced  
896 order constrained optimization (ROCO): Clinical application to lung IMRT,” *Med. Phys.* **38**,  
897 2731–2741, (2011).
- 898 <sup>25</sup> Y. Yang and M. J. Rivard, “Dosimetric optimization of a conical breast brachytherapy applicator  
899 for improved skin dose sparing,” *Med. Phys.* **37**, 5665–5671, (2010).
- 900 <sup>26</sup> X. Zhang, J. Wang, and L. Xing, “Metal artifact reduction in x-ray computed tomography (CT)  
901 by constrained optimization,” *Med. Phys.* **38**, 701–711, (2011).
- 902 <sup>27</sup> D. Butnariu, R. Davidi, G. T. Herman, and I. G. Kazantsev, “Stable convergence behavior under  
903 summable perturbations of a class of projection methods for convex feasibility and optimization  
904 problems,” *IEEE J. Sel. Top. Sign. Process.* **1**, 540–547, (2007).
- 905 <sup>28</sup> R. Davidi, G. T. Herman, and Y. Censor, “Perturbation-resilient block-iterative projection meth-  
906 ods with application to image reconstruction from projections,” *Int. Trans. Oper. Res.* **16**, 505–  
907 524, (2009).
- 908 <sup>29</sup> Y. Censor, R. Davidi, and G. T. Herman, “Perturbation resilience and superiorization of iterative  
909 algorithms,” *Inverse Probl.* **26**, 065008, (2010).
- 910 <sup>30</sup> T. Nikazad, R. Davidi, and G. T. Herman, “Accelerated perturbation-resilient block-iterative  
911 projection methods with application to image reconstruction,” *Inverse Probl.* **28**, 035005, (2012).
- 912 <sup>31</sup> G. T. Herman and R. Davidi, “Image reconstruction from a small number of projections,” *Inverse*  
913 *Probl.* **24**, 045011, (2008).
- 914 <sup>32</sup> E. Garduño, R. Davidi, and G. T. Herman, “Reconstruction from a few projections by  $\ell_1$ -

- 915 minimization of the Haar transform,” *Inverse Probl.* **27**, 055006, (2011).
- 916 <sup>33</sup> R. L. Rardin and R. Uzsoy, “Experimental evaluation of heuristic optimization algorithms: A  
917 tutorial,” *J. Heuristics* **7**, 261–304, (2001).
- 918 <sup>34</sup> L. Wernisch, S. Hery, and S. J. Wodak, “Automatic protein design with all atom force-fields by  
919 exact and heuristic optimization,” *J. Mol. Biol.* **301**, 713–736, (2000).
- 920 <sup>35</sup> S. H. Zanakis and J. R. Evans, “Heuristic optimization - why, when, and how to use it,” *Interfaces*  
921 **11**, 84–91, (1981).
- 922 <sup>36</sup> G. T. Herman and W. Chen, “A fast algorithm for solving a linear feasibility problem with  
923 application to intensity-modulated radiation therapy,” *Linear Algebra Appl.* **428**, 1207–1217,  
924 (2008).
- 925 <sup>37</sup> E. S. Helou Neto and Á. R. De Pierro, “Incremental subgradients for constrained convex opti-  
926 mization: A unified framework and new methods,” *SIAM J. Optimiz.* **20**, 1547–1572, (2009).
- 927 <sup>38</sup> E. S. Helou Neto and Á. R. De Pierro, “On perturbed steepest descent methods with inexact  
928 line search for bilevel convex optimization,” *Optimization* **60**, 991–1008, (2011).
- 929 <sup>39</sup> E. A. Nurminski, Envelope stepsize control for iterative algorithms based on Fejer processes with  
930 attractants, *Optimiz. Method. Softw.* **25**, 97–108, (2010).
- 931 <sup>40</sup> P. L. Combettes and J. Luo, “An adaptive level set method for nondifferentiable constrained  
932 image recovery,” *IEEE Trans. Image Proc.* **11**, 1295–1304, (2002).
- 933 <sup>41</sup> P. L. Combettes and J.-C. Pesquet, “Image restoration subject to a total variation constraint,”  
934 *IEEE Trans. Image Proc.* **13**, 1213–1222, (2004).
- 935 <sup>42</sup> E. Y. Sidky and X. Pan, “Image reconstruction in circular cone-beam computed tomography by  
936 constrained, total-variation minimization,” *Phys. Med. Biol.* **53**, 4777–4807, (2008).
- 937 <sup>43</sup> J. Bian, J. H. Siewerdsen, X. Han, E. Y. Sidky, J. L Prince, C. A. Pelizzari and X. Pan,  
938 “Evaluation of sparse-view reconstruction from flat-panel-detector cone-beam CT,” *Phys. Med.*  
939 *Biol.* **55**, 6575–6599, (2010).
- 940 <sup>44</sup> M. Defrise, C. Vanhove, and X. Liu, “An algorithm for total variation regularization in high-  
941 dimensional linear problems,” *Inverse Probl.* **27**, 065002, (2011).
- 942 <sup>45</sup> Y. Censor, W. Chen, P. L. Combettes, R. Davidi, and G. T. Herman, “On the effectiveness of  
943 projection methods for convex feasibility problems with linear inequality constraints,” *Comput.*  
944 *Optim. Appl.* **51**, 1065–1088, (2012).
- 945 <sup>46</sup> J. Bioucas-Dias and M. Figueiredo, “A new TwIST: two-step iterative shrinkage/thresholding

- 946 algorithms for image restoration,” *IEEE Trans. Image Proc.* **16**, 2992–3004, (2007).
- 947 <sup>47</sup> T. Goldstein and S. Osher, “The split Bregman method for L1 regularized problems,” *SIAM J.*  
948 *Imaging Sci.* **2**, 323–343, (2009).
- 949 <sup>48</sup> L. A. Shepp and Y. Vardi, “Maximum likelihood reconstruction for emission tomography,” *IEEE*  
950 *Trans. Med. Imag.* **1**, 113–122. (1982).
- 951 <sup>49</sup> E. Levitan and G. T. Herman, “A maximum a posteriori probability expectation maximization  
952 algorithm for image reconstruction in emission tomography,” *IEEE Trans. Med. Imag.* **6**:185–  
953 192, (1987).
- 954 <sup>50</sup> W. Jin, Y. Censor and M. Jiang, “A heuristic superiorization-like approach to bioluminescence  
955 tomography,” in *Proceedings of the International Federation for Medical and Biological Engi-*  
956 *neering (IFMBE)* (Springer-Verlag, 2012), to appear.
- 957 <sup>51</sup> H. M. Hudson and R. S. Larkin, “Accelerated image reconstruction using ordered subsets of  
958 projection data,” *IEEE Trans. Med. Imag.* **13**, 601–609, (1994).
- 959 <sup>52</sup> T. Elfving, “Block-iterative methods for consistent and inconsistent linear equations,” *Numer.*  
960 *Math.* **35**, 1–12, (1980).
- 961 <sup>53</sup> P. P. B. Eggermont, G. T. Herman, and A. Lent, “Iterative algorithms for large partitioned linear  
962 systems, with applications to image reconstruction,” *Linear Algebra Appl.* **40**, 37–67, (1981).
- 963 <sup>54</sup> R. Aharoni and Y. Censor, “Block-iterative projection methods for parallel computation of so-  
964 lutions to convex feasibility problems,” *Linear Algebra Appl.* **120**, 165–175, (1989).
- 965 <sup>55</sup> G. T. Herman, *Fundamentals of Computerized Tomography: Image Reconstruction from Projec-*  
966 *tions*, 2nd ed., Springer, 2009.
- 967 <sup>56</sup> J. F. P. J. Abascal, J. Chamorro-Servent, J. Aguirre, S. Arridge, T. Correia, J. Ripoli, J.  
968 J. Vaquero, and M. Desco, “Fluorescence diffuse optical tomography using the split Bregman  
969 method,” *Med. Phys.* **38**, 6275–6284, (2011)
- 970 <sup>57</sup> R. Davidi, G. T. Herman, and J. Klukowska, *SNARK09: A Programming System for the Re-*  
971 *construction of 2D Images from 1D Projections*, <http://www.snark09.com>, 2009.
- 972 <sup>58</sup> G. T. Herman and L. B. Meyer, “Algebraic reconstruction techniques can be made computa-  
973 tionally efficient,” *IEEE Trans. Med. Imag.* **12**, 600–609, (1993).
- 974 <sup>59</sup> W. Zbijewski and F. J. Beekman, “Characterization and suppression of edge and aliasing artefacts  
975 in iterative x-ray CT reconstruction,” *Phys. Med. Biol.* **49**, 145–157, (2004).